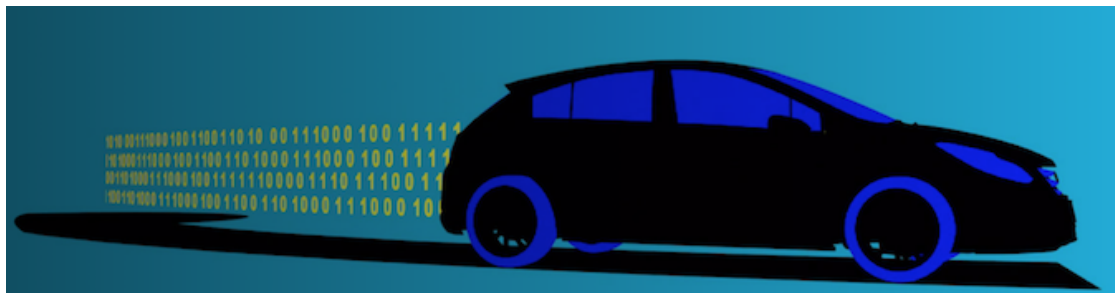


Master Thesis

Simulation of vehicle model for road features detection

B. Sc. Jinbo Chen



Reviewer: M.Sc. Johannes Masino

Nr.: 17-F-0114

Karlsruhe, November 2017

Master Thesis

Mr B. Sc. Jinbo Chen

(Std.-Nr.: 1791575)

Simulation of vehicle model for road features detection

Scope of the Thesis

The task of the research project is to detect the road features with data mining method in simulation environment.

The solution of this task is split into the following subtasks:

- Induction of the theme by researching about the current state of the art
- Implementation of different road surfaces and road damages.
- Further development of the full car model
- Extraciton of features for the Machine Learning.
- Training the Support-Vector Machine for the Machine Learning.
- Improving the classification for practical application
- Documentation of the entire work.

Hiermit wird die Vollständigkeit der Aufgabenstellung bestätigt. Alle darüber hinaus gehenden Aufgaben sind nicht Teil der Abschlussarbeit oder werden in der Ausarbeitung als solche kenntlich gemacht. Sollte es der/dem Studierenden, ohne eigenes Verschulden, nicht möglich sein, diese Aufgabenstellung in der vorgesehenen Bearbeitungszeit vollständig zu erfüllen, ist dies in der Ausarbeitung zu begründen. Mit ihrer/seiner Unterschrift nimmt die/der Studierende die Aufgabenstellung an. Der Ausgabe- sowie Abgabetag ist somit bindend

Ausgabetag: 01.08.17

Abgabetag: 30.11.17

Betreuer:

Projektleiter:

(Prof. Dr.rer.nat. Frank Gauterin)

(M.Sc. Johannes Masino)

Bearbeiter:

Anschrift:

(B. Sc. Jinbo Chen)

Klosterweg.28
76131 Karlsruhe, Germany
Tel.: 49-176-7266-9331

Erklärung zur Selbstständigkeit und wissenschaftlichen Praxis

Hiermit versichere ich, die Arbeit selbstständig verfasst und keine anderen als die angegebenen Quellen und Hilfsmittel benutzt sowie, die wörtlich oder inhaltlich übernommenen Stellen als solche kenntlich gemacht zu haben.

Die Satzung des Karlsruher Instituts für Technologie (KIT) zur Sicherung guter wissenschaftlicher Praxis in der jeweils gültigen Fassung habe ich beachtet.

Karlsruhe, den 30.11.2017

Kurzfassung

Simulation des Fahrzeugmodells zur Erkennung von Straßenmerkmalen

Der Zustand der Straßeninfrastruktur beeinflusst Wohlstand, Produktivität, Wachstum und soziales Wohlergehen moderner Volkswirtschaften. Die gegenwärtige Praxis der Straßenzustandsüberwachung ist mühsam und zeitaufwendig, da die meisten Schritte des Prozesses manuell durchgeführt werden. Nur wenige Länder verfügen über die teure Spezialfahrzeuge für eine automatisierte Datenerhebung. Außerdem die Überwachung ist nur in festen Intervallen von 1 bis 4 Jahren stattgefunden. Mit der gegenwärtigen Praxis ist es unmöglich, dass Defekte in die frühe Phase umfassend identifiziert werden, bis die Reparaturen kosteneffizienter sind. Vision-basierte Systeme können nur dann sehr umfassende Informationen liefern, wenn die Sichtlinie nicht behindert wird und genügend Rechenressourcen verfügbar sind. Daher wurden neue Verfahren auf der Basis von Fahrzeugsensoren, insbesondere ein Inertialsensor, in der Fahrzeugkarosserie und überwachtes maschinelles Lernen entwickelt, um die Straßeninfrastruktur automatisch zu überwachen. Überwachte maschinelle Lerntechniken beinhalten jedoch eine kostspielige und mühsame Sammlung von gelabelten Daten zum Trainieren und Testen. Wir haben eine neuartige Simulationsumgebung entwickelt, um diese Kosten zu reduzieren und spezifische Fahrzeugparameter und Einstellungen für die Klassifikationsergebnisse zu untersuchen und zu quantifizieren. Die entwickelten Simulationen und Ergebnisse ist hilfreich für die Verbesserung von dem Modell um den realen Anwendungen.

Abstract

Simulation of vehicle model for road features detection

The condition of the road infrastructure influences the prosperity, productivity, growth and social wellbeing of modern economies. Current practice of road condition monitoring is laborious and time-consuming as most steps of the process are done manually. Few countries have expensive specialized vehicles for an automated data collection whereas the monitoring is only scheduled in fixed intervals of 1 to 4 years. With current practice defects are unlikely to be comprehensively identified in early stages, when repairs are more cost-efficient. Vision-based systems can provide very comprehensive information only when the line of sight is not obstructed and enough computational resources are available. Therefore, new methods based on vehicle sensors, especially an inertial sensor, in the vehicle body, and supervised machine learning have been developed to autonomously monitor the road infrastructure. However, supervised machine learning techniques involve a costly and laboriously collection of labeled data for training and testing. We have developed a novel simulation environment to reduce these costs and to investigate and quantify specific vehicle parameters and settings on the classification results. The developed simulation and results help to improve the models for real world applications.

Danksagung

An dieser Stelle möchte ich mich bei all denjenigen bedanken, die mich während der Anfertigung dieser Masterarbeit unterstützt und motiviert haben.

Zuerst gebührt mein Dank Herr Johannes Masino, der meine Masterarbeit betreut und begutachtet hat und mir mit viel Geduld, Interesse und Hilfsbereitschaft zur Seite standen. Für die hilfreichen Anregungen, die konstruktive Kritik bei der Erstellung dieser Arbeit möchte ich mich herzlich bei ihm bedanken, ohne die diese Arbeit nicht hätte entstehen können.

Ebenfalls möchte ich mich bei Herrn Prof. Frank Gauterin und Herrn Dr. Michael Frey bedanken, die mich mit allen seinen Mitteln unterstützten und ohne dessen Hilfe und Bemühungen diese Arbeit nicht zustande gekommen wäre.

Meinen Freunden Oliver, Zhe Pang und meiner Freundin Hui Wang danke ich besonders für den Hilfen und starken emotionalen Rückhalt über die Dauer meines gesamten Studiums.

Abschließend möchte ich mich bei meinen Eltern bedanken, die mir mein Studium durch ihre Unterstützung ermöglicht haben und stets ein offenes Ohr für meine Sorgen hatten.

Jinbo Chen,

Karlsruhe, 26.11.2017

Contents

Kurzfassung	v
1. Simulation des Fahrzeugmodells zur Erkennung von Straßenmerkmalen	v
Abstract	vi
1. Simulation of vehicle model for road features detection	vi
Danksagung	vii
Glossary	x
1. Introduction	1
2. Simulation	3
2.1. Road model	3
2.2. Basic full car model	4
2.3. Transfer function of the Full Car Model	9
2.4. Full car model with anti-roll bar	13
2.5. Full car model with active suspension	14
2.6. Position of output	22
2.7. Tire model	23
2.7.1. Rigid Ring Model	25
2.7.2. Modified Point Contact Tire Model	28
3. Identification and validation	30
3.1. Identification and validation of the damping ratio	30
3.2. Identification and validation of the tire model	33
4. Methodology	36
4.1. Data processing	36
4.2. Road events and data labelling	38
4.3. Feature extraction	39
4.4. Display and evaluation of the classification	39

4.5. Variation of simulation	41
5. Implementation	43
5.1. Introduction of the software	43
5.2. Explanation of the scripts in MATLAB	44
5.3. Working with SCIXMINER	47
6. Results	50
6.1. Variation of vehicle parameters	50
6.1.1. Classification accuracy	50
6.1.2. Feature selection	52
6.1.3. Application of the classifier	53
6.2. Variation of simulation	55
7. Summary and outlook	59
A. List of Figures	61
B. List of Tables	63
Bibliography	64

Glossary

ABS Antiblockiersystem

DGL Differentialgleichung

SPD spectral power distribution

PSD power spectral density

IRI international roughness index

FCM full car model

DOF degrees of freedom

LQR linear quadratic regulator

SVFB state-variable feedback

SISO single-input single-output

MIMO multi-input multi-output

MANOVA multivariate analysis of variance

SVM support vector machine

LDA linear discriminant analysis

intBP integration of the band-pass filter for a certain frequency range

maxBP maximum of the band-pass filter for a certain frequency range

Std standard deviation

RMS root mean square

SNR signal to noise ration

1. Introduction

The condition of the road infrastructure has severe impacts on the driving comfort, driving safety, tire road noise and rolling resistance [11, 17, 23, 36]. Subsequently, tire road noise leads to sleep disturbances, general annoyance, or speech interference [32, 38]. Therefore the costs for noise abatement measures increases [7] and the value of houses and land close to noisy transport roads decreases [42, 43, 47]. A higher rolling resistance leads to higher vehicle operational costs, e.g. for fuel, and decreases the range of electric vehicles [5]. Furthermore, a delayed detection and maintenance of road damages results in the erosion of the road substance. Subsequently, a complete renewal increases the costs over the life cycle of the road and yields to a complete roadblock and traffic jams [14]. State departments of transport around the world mainly monitor the road infrastructure manually, which is laborious and time-consuming [34]. Inspectors collect data manually and rate road segments based on their experience. Only few countries employ specialized vehicles with an automated data collection [22]. However, they are sophisticated and expensive to use [34].

Researches have addressed the common problem of road infrastructure monitoring and present methods, which are based on vehicle sensors and machine learning. The idea is to collect data with a crowd of vehicles with on-board sensors, which sense the environment of the vehicle [33]. A literature review about this approach is given in [33]. The most promising sensors are cameras, such as the Bosch stereo camera, or inertial sensors in the vehicle body.

Novel developed computer vision techniques lead to good results of the detection of road defects. However, only high class vehicles with expensive packages, e.g. magic body control from Mercedes-Benz, have a camera on-board. Moreover, they are limited to decent weather conditions and higher velocities of the vehicle have a negative impact on the precision [33]. Furthermore, computer vision needs a lot of storage and computer power since a large amount of data need to be processed.

In contrast to cameras, the inertial sensors are less computational intensive and independent from light conditions. Several studies have shown that inertial sensor data from the vehicle body with data processing based on machine learning are suitable to detect road damages or estimate the road roughness [9, 13, 30, 31, 39]. Most papers implement a classification, which predicts specific

road defects, such as potholes. The classifier is trained with inertial sensor data labeled with the desired output, here the road defects. After the training process, the classifier is tested with new and unseen labeled data. The output of the training and testing process are confusion matrices, from which performance measures can be derived, e.g. the accuracy, precision and recall. However, only few kilometres and specific road segments with few variations of the driving conditions are applied in most papers. More importantly, no study has performed a sensitivity analysis and has investigated the impact of different influences on the classification accuracy, e.g. the vehicle load, noise of the sensor, or the type of vehicle.

This research cap is closed and a novel simulation environment is presented, which is based on a full car model. The road features, such as potholes, railroad crossing are simulated with functions and those contact with tires is also considered. In this thesis, a basic full car model is enhanced to analyze the impact of different settings of the vehicle on the classification results of road defects. The road is modeled as a surface with different degrees of roughness and the spectral power distribution (SPD) of our road corresponds to the SPD of real road surfaces. Furthermore, the position of the inertial sensor in the vehicle is varied in the simulation to identify the position with highest signal-to-noise ratio and which leads to the best classification accuracy.

The advantage of this novel environmental simulation in contrast to real test drives is the reproducibility and the precise investigation of specific influences. Furthermore, the costs to perform this analysis is drastically reduced. The results of our investigations helps the further development of automatic road condition monitoring system and reduces the efforts to investigate further influences or to test novel classification algorithms.

2. Simulation

2.1. Road model

In general, the unevenness density of a road real profile decreases with an increase in spatial frequency. The SPD of a road profile is defined in [1] as

$$G_d(\Omega) = \begin{cases} G_d(\Omega_0) \cdot \left(\frac{\Omega}{\Omega_0}\right)^{-n_1} & \text{if } \Omega \leq \frac{1}{2\pi} \\ G_d(\Omega_0) \cdot \left(\frac{\Omega}{\Omega_0}\right)^{-n_2} & \text{if } \Omega > \frac{1}{2\pi} \end{cases}, \quad (2.1)$$

where $\Omega = \frac{2\pi}{L}$ is the angular spatial frequency and L the road length. Usually, $n_1 = 2$, $n_2 = 1.5$, $\Omega_0 = 1$ and the degree of roughness $G_d(\Omega_0)$ can be obtained from [1] for different road classes. It ranges from 0 (very smooth) to 8192 (very bad condition). The unit of $G_d(\Omega_0)$ is $10^{-6}m^3$ and the unit of Ω_0 is rad/m . A random periodic road profile that fits the SPD described in (2.1) can be generated with a Fourier series, the sum of individual sine waves, with [3, 8].

$$r(x) = \sum_{i=0}^N \hat{p}_i \cdot \sin(2\pi \cdot i \cdot x + \epsilon_i), \quad (2.2)$$

which lead us to

$$r(x) = \sum_{i=0}^N \sqrt{2 \cdot \Delta\Omega \cdot G_d(i \cdot \Delta\Omega)} \cdot \sin(2\pi \cdot i \cdot x \cdot \Delta\Omega + \epsilon_i). \quad (2.3)$$

$\Delta\Omega$ is the frequency band and ϵ_i as a random phase angle uniformly distributed between 0 and 2π .

Furthermore, we have added road features to our road profile, including potholes, manhole cover, railway crossing and cobbled road. It is described through suitable functions with varying parameters in a specific range, e.g. the depth or height h and the length l of such road features. Hereby, an

obstacle described by a non-continuously differentiable function can cause numerical issues in the time step integration process of the simulation itself [15]. Thus the transition part of the road features should be smooth. The function and the profile of the road features are shown as below.

$$f_{\text{pothole}}(x) = \frac{h}{2} \cdot (\cos(\frac{2\pi}{l} \cdot x) - 1) \quad (0 \leq x \leq l), \quad (2.4)$$

$$f_{\text{manhole_cover}}(x) = \begin{cases} \frac{h}{2} \cdot (1 - \cos(\frac{12\pi}{l} \cdot x)) & (0 \leq x \leq \frac{l}{12}) \\ 1 & (\frac{l}{12} \leq x \leq \frac{11l}{12}) \\ \frac{h}{2} \cdot (1 + \cos(\frac{12\pi}{l} \cdot (x - \frac{11l}{12}))) & (\frac{11l}{12} \leq x \leq l) \end{cases}, \quad (2.5)$$

$$f_{\text{cobble_left}}(x) = \frac{h}{2} \cdot (1 - \cos(\frac{2\pi}{l} \cdot x)) \quad (0 \leq x \leq l), \quad (2.6)$$

$$f_{\text{cobble_right}}(x) = \frac{h}{2} \cdot (1 + \cos(\frac{2\pi}{l} \cdot x)) \quad (0 \leq x \leq l), \quad (2.7)$$

$$f_{\text{railway_crossing}}(x) = \begin{cases} \frac{h}{2} \cdot (\cos(\frac{80\pi}{l} \cdot x) - 1) & (0 \leq x \leq \frac{l}{80}) \\ 0 & (\frac{l}{80} \leq x \leq \frac{l}{16}) \\ \frac{h}{2} \cdot (\cos(\frac{80\pi}{l} \cdot (x - \frac{5l}{80})) + 1) & (\frac{5l}{80} \leq x \leq \frac{6l}{80}) \\ 0 & (\frac{6l}{80} \leq x \leq \frac{74l}{80}) \\ \frac{h}{2} \cdot (\cos(\frac{80\pi}{l} \cdot (x - \frac{74l}{80})) - 1) & (\frac{74l}{80} \leq x \leq \frac{75l}{80}) \\ 0 & (\frac{75l}{80} \leq x \leq \frac{79l}{80}) \\ \frac{h}{2} \cdot (\cos(\frac{80\pi}{l} \cdot (x - \frac{79l}{80})) + 1) & (\frac{79l}{80} \leq x \leq l) \end{cases}. \quad (2.8)$$

Fig. 2.1 shows the generated road profile, which is used to show the influences of various extensions of the full car model in Sections 2.4 to 2.6.

2.2. Basic full car model

The basic full car model consists of springs, dampers, masses and incorporates pitch and roll motion, giving a total of seven degrees of freedom (DOF). Consequently it can present more details of the behavior of the vehicle traversing different road situation. The mass of axle is distributed to the vehicle body and the mass of the wheel and tire is modeled as a mass point. To simplify the calculation, the roll center and pitch center of the vehicle are assumed to coincide in the gravity center. Besides, we set 1, 2 as the front-right and front-left wheel and 3, 4 as the rear-right and rear-left wheel.

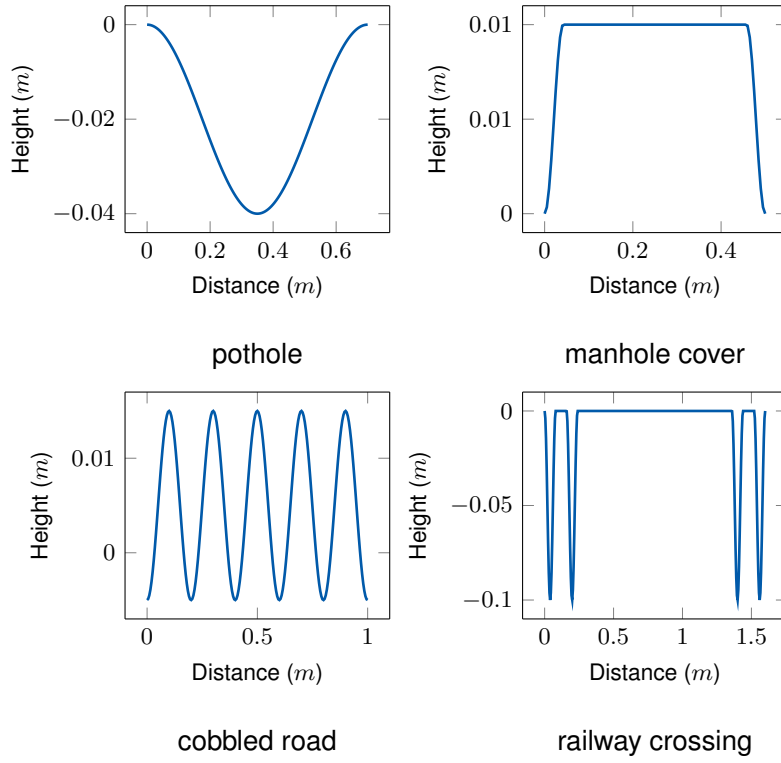


Figure 2.1.: Generated road profile for simulation of car models described in Sections 2.4 to 2.6. Left and right profiles are different to investigate the influence of the anti-roll bar.

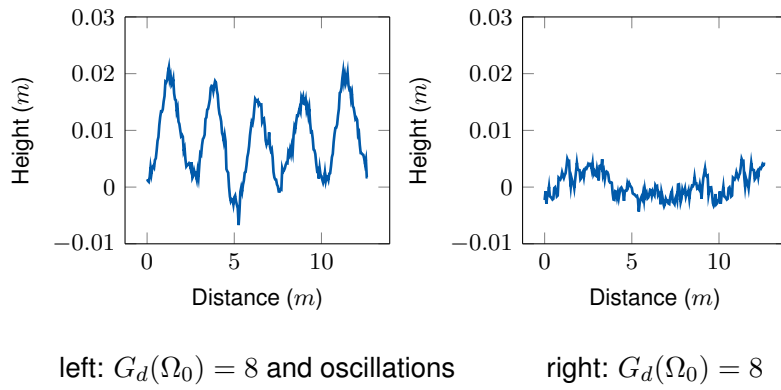


Figure 2.2.: Generated road profile for simulation of car models described in Sections 2.4 to 2.6. Left and right profiles are different to investigate the influence of the anti-roll bar.

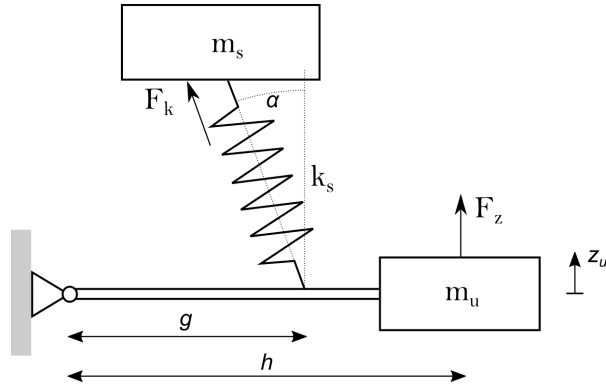


Figure 2.3.: The strut equivalent schematic

Since the damper of the tire is very small compared to the damper of the suspension, it can be neglected. A damper limits the resonant response of the vehicle vibration due to the suspension springs is non-linear. However, the transmission behavior of the axis has improved its linearity until the wheel frequency due to the interaction between the ripple of the roadway excitation and the transfer behavior of the axis. This advocates the use of linear transfer functions to characterize the vibration comfort [18]. Thus the passive suspension system between the sprung mass and unsprung masses was modeled as a linear spring and viscous damper at each corner.

The front suspension of the test vehicle BMW 116d is the MacPherson suspension and the rear suspension of it is multi-link suspension. It is well known that the strut of these suspension is not directly connected to the center of the tire. Moreover, the strut of the MacPherson suspension especially has an angle relative to the vertical line of the tire. The method to describe the suspension can be found in [20], which is shown in Fig. 2.3.

Regardless of the damper, the spring elongation δ_u is

$$\delta_u = -\frac{g}{h} \cos \alpha \cdot z_u \quad (2.9)$$

According to the spring elongation, the spring force F_k is

$$F_k = -k_s \delta_u = k_s \frac{g}{h} \cos \alpha \cdot z_u \quad (2.10)$$

It is now possible to substitute the tilted spring elongation with an equivalent spring elongation z_{eq} on the z-axis that needs the same force F_z , to elongate the same amount as the mass moves.

Table 2.1.: Definition of the variables

variables	definition
z	vertical displacement of the vehicle body
z_{si}	vertical displacement of the i th sprung mass
z_{ui}	vertical displacement of the i th unsprung mass

$$z_{eq} = \frac{g}{h} \cos \alpha \cdot z_u \quad (2.11)$$

The vertical component of the force on the unsprung mass can be calculated by

$$F_z = \frac{g}{h} \cos \alpha \cdot F_k \quad (2.12)$$

Thus the relationship can be describe by a equivalent coefficient i , the force on the sprung mass F and on the unsprung mass F_z are

$$F = -\cos \alpha \cdot (k_s(z_s - i \cdot z_u) + d_s(\dot{z}_s - i \cdot \dot{z}_u)) \quad (2.13)$$

$$F_z = i \cdot (k_s(z_s - i \cdot z_u) + d_s(\dot{z}_s - i \cdot \dot{z}_u)) \quad (2.14)$$

where

$$i = \frac{g}{h} \cos \alpha \quad (2.15)$$

The equivalent coefficient i is relative to the dimension of the structure of the suspension. Due to the unavailable devices for the measurement of the length and angle of the strut, the coefficient is temporarily assumed as one. Here i ignore the influence by the mechanic structure of the suspension.

With the above mentioned assumptions the full car model (FCM) is shown in Fig. 2.4,

The definition of the not labeled variables is shown in table 2.1 and the differential equations of the heaving (2.16), pitching (2.17), rolling (2.18) of the vehicle and vertical motion of each wheel (2.19) is derived as follows

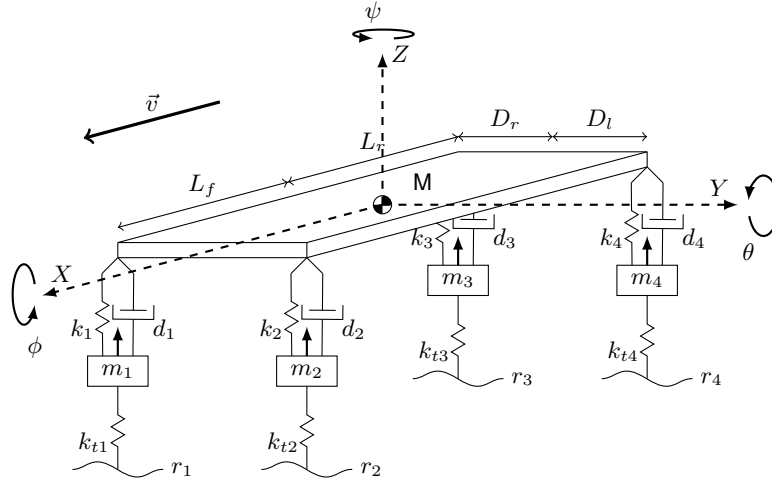


Figure 2.4.: Full car model for simulation.

$$M\ddot{z} = \sum_{i=1}^4 -k_i(z_{si} - z_{ui}) - d_i(\dot{z}_{si} - \dot{z}_{ui}), \quad (2.16)$$

$$J_{yy}\ddot{\theta} = \sum_{i=1,2} D_f(k_i(z_{si} - z_{ui}) + d_i(\dot{z}_{si} - \dot{z}_{ui})) + \sum_{i=3,4} -D_r(k_i(z_{si} - z_{ui}) + d_i(\dot{z}_{si} - \dot{z}_{ui})), \quad (2.17)$$

$$J_{xx}\ddot{\phi} = \sum_{i=1,3} L_l(k_i(z_{si} - z_{ui}) + d_i(\dot{z}_{si} - \dot{z}_{ui})) + \sum_{i=2,4} -L_r(k_i(z_{si} - z_{ui}) + d_i(\dot{z}_{si} - \dot{z}_{ui})), \quad (2.18)$$

$$m_i\ddot{z}_{ui} = k_i(z_{si} - z_{ui}) + d_i(\dot{z}_{si} - \dot{z}_{ui}) - k_{ti}(z_{ui} - r_i). \quad (2.19)$$

The relation between z and z_{si} is

$$z_{s1} = z - L_f\theta + D_l\phi, \quad (2.20)$$

$$z_{s2} = z - L_f\theta - D_r\phi, \quad (2.21)$$

$$z_{s3} = z + L_r\theta + D_l\phi, \quad (2.22)$$

$$z_{s4} = z + L_r\theta - D_r\phi. \quad (2.23)$$

The differential equations are transferred into state space representation, which is a compact

mathematical model of a physical system as a set of input, output and state variables related by first-order differential equations. It replaces n order linear differential equations with a first order matrix differential equation, directly provides a time-domain solution, and is computational efficient.

$$\dot{x} = Ax + Bu \quad (2.24)$$

$$y = Cx + Du \quad (2.25)$$

where x is a 14×1 state vector which contains the first and second derivative of the vertical, roll and pitch motion, u a 4×1 input vector containing the road signal of each wheel. The output variable y is a 3×1 vector that contains the response of the vehicle body at vertical, roll and pitch direction. The dynamic system is simulated in MATLAB with the Control System Toolbox.

2.3. Transfer function of the Full Car Model

The transfer function is a mathematical function giving the corresponding output value for each possible value of the input to the system. It is a good way to simplify the behavior of the vehicle to the road signal, because it is identified only by the the road signal and the accelerations of the vehicle [18]. With the Laplace-Transformation the model can be transferred from state space to transfer function.

$$sX(s) = AX(s) + BU(s) \quad (2.26)$$

$$Y(s) = CX(s) + DU(s) \quad (2.27)$$

transformed with $X(s)$, the transfer function $G(s)$

$$X(s) = (s \cdot I - A)^{-1} \cdot B \cdot U(s) \quad (2.28)$$

$$Y(s) = (C \cdot (s \cdot I - A)^{-1} \cdot B + D) \cdot U(s) \quad (2.29)$$

$$G(s) = C \cdot (s \cdot I - A)^{-1} \cdot B + D \quad (2.30)$$

The element at i th row and j th column in the transfer function $G(s)$ is the also the sub transfer function of the i th output and the j th input.

$$G_{ij} = \frac{Y_i}{U_j} \quad (2.31)$$

Hence the full car model can be described as

$$\begin{bmatrix} \ddot{Z} \\ \ddot{\Theta} \\ \ddot{\Phi} \end{bmatrix} = \begin{bmatrix} G_{11} & G_{12} & G_{13} & G_{14} \\ G_{21} & G_{22} & G_{23} & G_{24} \\ G_{31} & G_{32} & G_{33} & G_{34} \end{bmatrix} \cdot \begin{bmatrix} R_1 \\ R_2 \\ R_3 \\ R_4 \end{bmatrix} \quad (2.32)$$

In this multi-input multi-output (MIMO) system which has four inputs and three outputs, the lift, pitch and roll motion of the vehicle are resulted by the multiplication of each transfer function G_{ij} and the corresponding road stimulation r_j . Because the value of the variables of the four subset e.g k_i , d_i and k_{ti} in the vehicle suspension are symmetrically, after the calculation in formular 2.30, the amplitude of the sub transfer function in the same row are consequently identical but some phases are shifted. The bode phase plot of all the sub transfer functions are shown in Fig. 2.3. The row indicates the four inputs and the column indicates the three outputs.

It can be seen that the profile of the phase plots in the same column are identical. Besides, the phase of several outputs have a -180° translation, which means those outputs should take the opposite values. To simplify the transfer function, we set three new inputs from the combination of the four road signals to match the phase plot of sub transfer functions.

The input for the heaving motion is the sum of all signals.

$$U_{heave} = r_1 + r_2 + r_3 + r_4 \quad (2.33)$$

The input for the pitching motion is the difference of front axle and rear axle

$$U_{pitch} = r_1 + r_2 - r_3 - r_4 \quad (2.34)$$

The input for the rolling motion is the difference of left side and right side

$$U_{roll} = r_1 - r_2 + r_3 - r_4 \quad (2.35)$$

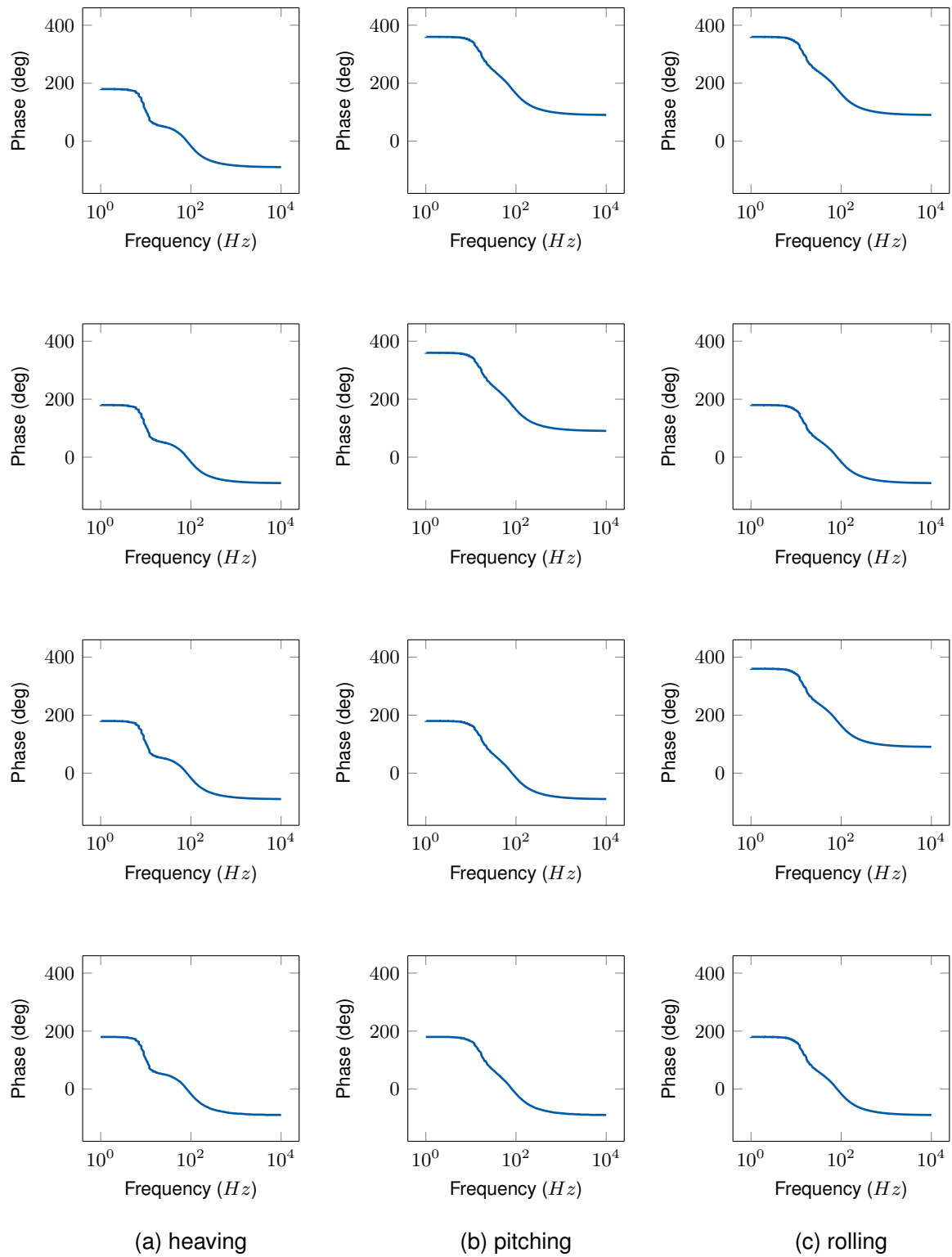


Figure 2.5.: Bode Phase Plot of All Transfer Functions.

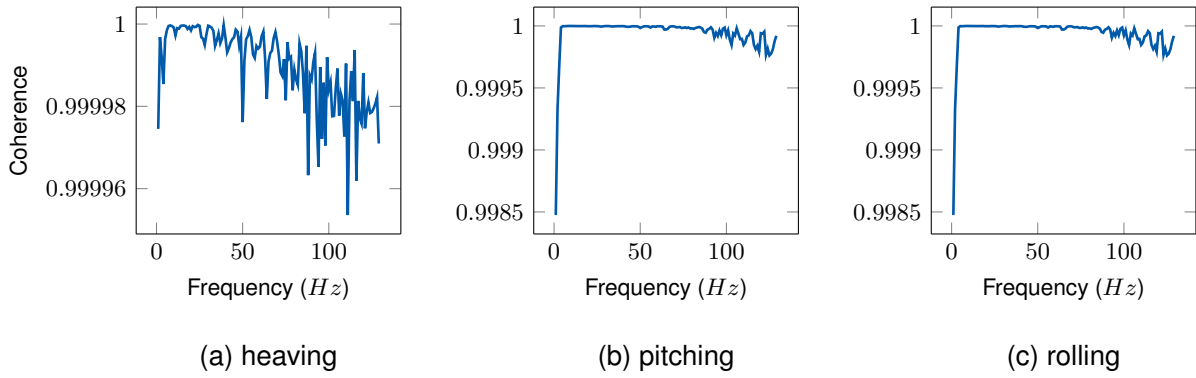


Figure 2.6.: Coherence of the response between MIMO- and SISO system

With the new inputs and transfer functions the MIMO system is transformed to three single-input single-output (SISO) systems.

$$\begin{bmatrix} \ddot{Z} \\ \ddot{\Theta} \\ \ddot{\Phi} \end{bmatrix} = \begin{bmatrix} G_z & 0 & 0 \\ 0 & G_p & 0 \\ 0 & 0 & G_r \end{bmatrix} \cdot \begin{bmatrix} U_{heave} \\ U_{pitch} \\ U_{roll} \end{bmatrix} \quad (2.36)$$

where

$$G_z = G_{11} \quad (2.37)$$

$$G_p = G_{21} \quad (2.38)$$

$$G_r = G_{31} \quad (2.39)$$

Fig. 2.3 shows the coherence between the response of the MIMO system and SISO system with the road profile in 2.1. From the high coherence it is obvious that the results of two systems are almost identical. With this method state space representation has been converted to three SISO transfer function. This conversion makes the analysis of the feature of the full car model in frequency domain easier and can help us to analysis the relation between single output and all the inputs from the four wheels. It will be used in section 2.4 and 2.6.

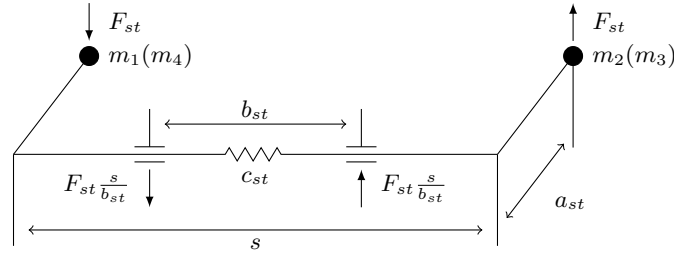


Figure 2.7.: Model of anti-roll bar as a torsion bar between two unsprung masses.

2.4. Full car model with anti-roll bar

An anti-roll bar, known also as a sway bar, is a commonly used automotive suspension component that elastically couples the suspension on one side of a vehicle to the adjacent side [12]. It helps to reduce the body roll of a vehicle when the deflection of body and tire between left and right side has a great difference [18]. A sway bar increases the suspension's roll stiffness to rolling motion and is independent of its spring rate in the vertical direction. Therefore, the influence of the anti-roll bar should be considered into the full car model. The model is shown in Fig. 2.7.

It connects left and right wheels together through short lever arms linked by a torsion spring whose stiffness is indicated as c_{st} . The force F_{st} is generated by anti-roll bar to the tire at front and rear axle (2.40) and anti-roll moment M_{st} to the body (2.41) are:

$$F_{st,f} = \pm \frac{c_{st,f}}{a_{st,f}^2} (z_{s1} - z_{u1} - z_{s2} + z_{u2}) \quad (2.40)$$

$$F_{st,r} = \pm \frac{c_{st,r}}{a_{st,r}^2} (z_{s3} - z_{u3} - z_{s4} + z_{u4}),$$

$$M_{st} = s \frac{c_{st}}{a_{st}^2} (z_{s1} - z_{u1} - z_{s2} + z_{u2}) + s \frac{c_{st}}{a_{st}^2} (z_{s3} - z_{u3} - z_{s4} + z_{u4}). \quad (2.41)$$

According to the additional forces and moments generated by the anti-roll bar, the rolling motion of the vehicle body (2.42) and vertical motion of each wheel (2.43) should be reformed:

$$J_{xx} \ddot{\phi} = -M_{st} + \sum_{i=1,3} -L_l (k_i (z_{si} - z_{ui}) + d_i (\dot{z}_{si} - \dot{z}_{ui})) + \sum_{i=2,4} L_r (k_i (z_{si} - z_{ui}) + d_i (\dot{z}_{si} - \dot{z}_{ui})), \quad (2.42)$$

$$m_i \ddot{z}_{ui} = k_i (z_{si} - z_{ui}) + d_i (\dot{z}_{si} - \dot{z}_{ui}) - k_{ti} (z_{ui} - r_i) + F_{st,i}. \quad (2.43)$$

Table 2.2.: Parameter of the simulation

L	D	M	k	d	m_{tire}	k_{tire}	a_{st}	c_{st}
$[m]$	$[m]$	$[kg]$	$[N/m]$	$[N \cdot s/m]$	$[kg]$	$[N/m]$	$[m]$	$[N \cdot m]$
2.69	1.71	1400	150000	2500	22.5	36689/35902	0.2	100

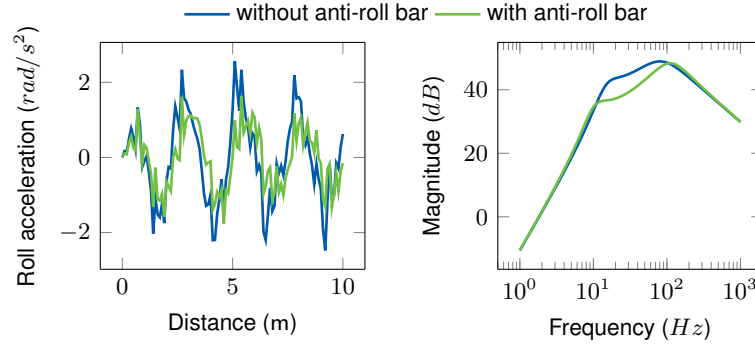


Figure 2.8.: Influence of the anti-roll bar. The roll acceleration is distinct reduced as well as the magnitude of the transfer function for lower frequencies.

The comparison of the response and transfer function which is already introduced in Sec. 2.3 from road deflection u_{roll} to body roll acceleration $\ddot{\phi}$ of the full car model without and with anti-roll bar are shown in Fig. 2.8. The setting of parameters in those simulations are shown in table 2.2.

It indicates that the roll acceleration is reduced and the magnitude of the transfer function is lower in the range from 10 to 100 Hz with the influence of the anti-roll bar. That is to say, the results of the simulation of rolling motion with the full car model without the anti-roll bar may be stretched. For the reliability and accuracy of the simulation, we add the anti-roll bar to the full car model.

2.5. Full car model with active suspension

In addition to the passive suspension with basic springs and dampers, active suspensions use separate actuators between the chassis and wheel assembly, which can exert an independent force on the suspension in order to improve the driving comfort.

Ideally, a control action may be introduced at different levels of the suspension system: at the level of the dissipative unit, by a modulation of the damping force; at the level of the elastic unit, by a modulation of the spring force; at the full level of the suspension, by replacing both the elastic and the damping devices with a force actuator. More specifically, three features may be observed: the control ability range which is the range of forces that the actuators can deliver; the control bandwidth

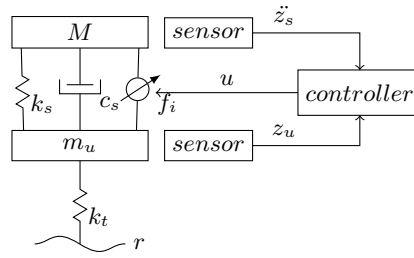


Figure 2.9.: One fourth of the full car model with active suspension.

which is a measure of how fast the actuator action is; the power request that is mainly due to the mix of control ability range and control bandwidth [37].

Due to the relatively vast range of deliverable forces, in principle, active suspensions may provide the best performance. The active suspension is characterized by its ability to use external energy and usually involves hydraulic components.

One fourth of the full car model with active suspension is shown in Fig. 2.9. The force f_i applied between the body and wheel assembly is generated by a hydraulic actuator and controlled by the feedback in the closed loop.

With this model the mathematical modeling for heaving (2.44), pitching (2.45), rolling (2.46) of the vehicle body and vertical motion of each wheel (2.47) is derived as follows:

$$M\ddot{z} = \sum_{i=1}^4 -k_{ui}(z_{si} - z_{ui}) - c_{ui}(\dot{z}_{si} - \dot{z}_{ui}) + f_i, \quad (2.44)$$

$$J_{yy}\ddot{\theta} = \sum_{i=1,2} L_f(k_{ui}(z_{si} - z_{ui}) + c_{ui}(\dot{z}_{si} - \dot{z}_{ui}) - f_i) + \sum_{i=3,4} -L_r(k_{ui}(z_{si} - z_{ui}) + c_{ui}(\dot{z}_{si} - \dot{z}_{ui}) - f_i), \quad (2.45)$$

$$J_{xx}\ddot{\phi} = \sum_{i=1,3} D_l(k_{ui}(z_{si} - z_{ui}) + c_{ui}(\dot{z}_{si} - \dot{z}_{ui}) - f_i) + \sum_{i=2,4} -D_r(k_{ui}(z_{si} - z_{ui}) + c_{ui}(\dot{z}_{si} - \dot{z}_{ui}) - f_i), \quad (2.46)$$

$$m_i\ddot{z}_{ui} = k_{ui}(z_{si} - z_{ui}) + c_{ui}(\dot{z}_{si} - \dot{z}_{ui}) - k_{ti}(z_{ui} - r_i) - f_i. \quad (2.47)$$

There has been a lot of research in the design of a suitable control strategy for the active suspension. For instance, in [10] three different control designs, PI, linear quadratic regulator (LQR) and H_∞

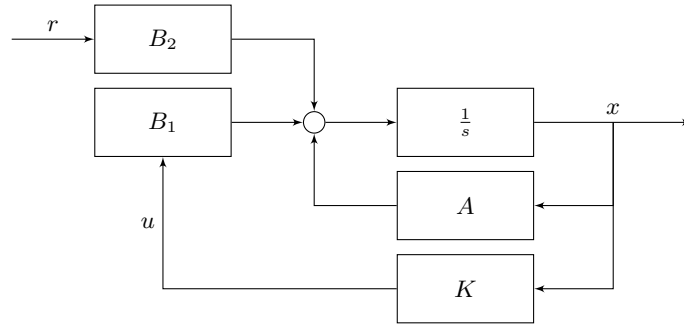


Figure 2.10.: Block diagram of the LQR.

were compared for stability, performance and robustness. Different advanced controllers have also been compared in several studies such as [21] and [35], where LQR, Fuzzy, Skyhook and H_∞ controllers were tested.

The LQR approach of vehicle suspension control is widely used in background of many studies in vehicle suspension control. The strength of LQR approach is that in using it the factors of the performance index can be weighted according to the designer's desires or other constraints [2].

The system can be expressed in the state space representation. State variable $x(t)$ is a 14×1 vector, input variable u is a 4×1 vector which contain the road signal of each wheels and f is the generated forces by actuator under the controller.

$$\dot{x}(t) = Ax(t) + B_1u(t) + B_2r(t) \quad (2.48)$$

It is assumed that all the states are measurable and consider a state-variable feedback (SVFB) regulator for the system as $u(t) = -Kx(t)$. With the state feedback gain matrix K the closed-loop system is reformed as

$$\dot{x}(t) = (A - B_1K)x(t) + B_2r(t) \quad (2.49)$$

The block diagram of the system is shown in Fig. 2.10. Set $A_c = A - B_1K$ and $B_c = B_2$, the system can be presented in state space as

$$\dot{x}(t) = A_cx(t) + B_cr(t) \quad (2.50)$$

$$y(t) = Cx(t) + Dr(t) \quad (2.51)$$

The optimal controller of given system is defined as controller design which minimizes the following cost-function.

$$J = \frac{1}{2} \int_0^{\infty} (x(t)^T Q x(t) + u(t)^T R u(t)) dt \quad (2.52)$$

Linear optimal control theory provides the solution of Eq. 2.52. The gain matrix K is computed from,

$$K = R^{-1} B_1^T P \quad (2.53)$$

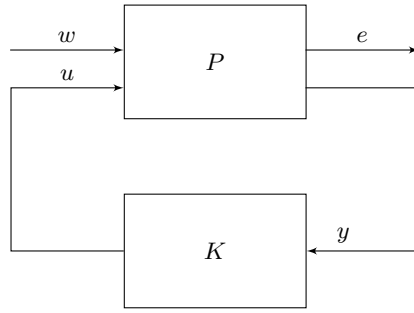
There are a numerical procedures for solving the restrictions. MATLAB routine that performs this operation is $lqr(A, B, Q, R)$.

where Q and R are positive definite weighting matrices. The two matrices are selected by the design engineer. There are a numerical procedures for solving the restrictions. MATLAB routine that performs this operation is $lqr(A, B, Q, R)$. Depending on how these design parameters are selected, the closed-loop system will exhibit a different response. Larger values of Q generally result in the poles of the closed-loop system matrix A_c being further left in the s-plane so that the state decays faster to zero. larger R means that less control effort is used, so that the poles are generally slower, resulting in larger values of the state $x(t)$ [2].

With the new state space representation we can build the model of the FCM with active suspension using the LQR controller.

However, since much of the intuitive insight about the effects of controller parameter modification gets lost in the LQR designs, the methods include no robustness specification. It was shown in [35] that the H_{∞} control design yields a superior controller that has significantly better stability and performance robustness as compared to classical designs as the design takes the performance specifications into account through the weighting functions. Most often the H_{∞} based methods have achieved the best results and point out that the efficiency of H_{∞} control theory seems to be a good choice for active suspension control, which is widely used in the automotive industry because of its low cost and simplicity [37]. Hence the H_{∞} controller is implemented as the force controller in the full car model with active suspension.

H_{∞} control is design in term of feasibility of certain delay dependent matrix inequalities. It confirms that H_{∞} control of active suspension system using the optimization of either a weighted single objective functional with hard constrains or multi-objective functional is an effective way to deal with the conflicting vehicle suspension performance problem [40].

Figure 2.11.: Control configuration of H_∞ control.

H_∞ control is formulated using the general control configuration in Fig. 2.11 where $P(s)$ is a linear system given as follows:

$$\begin{bmatrix} e \\ y \end{bmatrix} = \begin{bmatrix} P_{11} & P_{12} \\ P_{21} & P_{22} \end{bmatrix} \begin{bmatrix} w \\ u \end{bmatrix} \quad (2.54)$$

where w is the exogenous input vector, u is the control input vector, e is the controlled output vector and y is the measurement vector. The control design is to find a controller $K(s)$ for a generalized plant $P(s)$ such that, based on the information given by y , the control signal $u = K(s)y$ ensures internal stability of the closed-loop system and counteracts the influence of w on e , thereby minimizing the closed-loop transfer norm from the exogenous inputs w to the controlled outputs e [35].

Given γ , a prespecified attenuation level. The H_∞ control is to design a controller that internally stabilizes the closed-loop system and ensures:

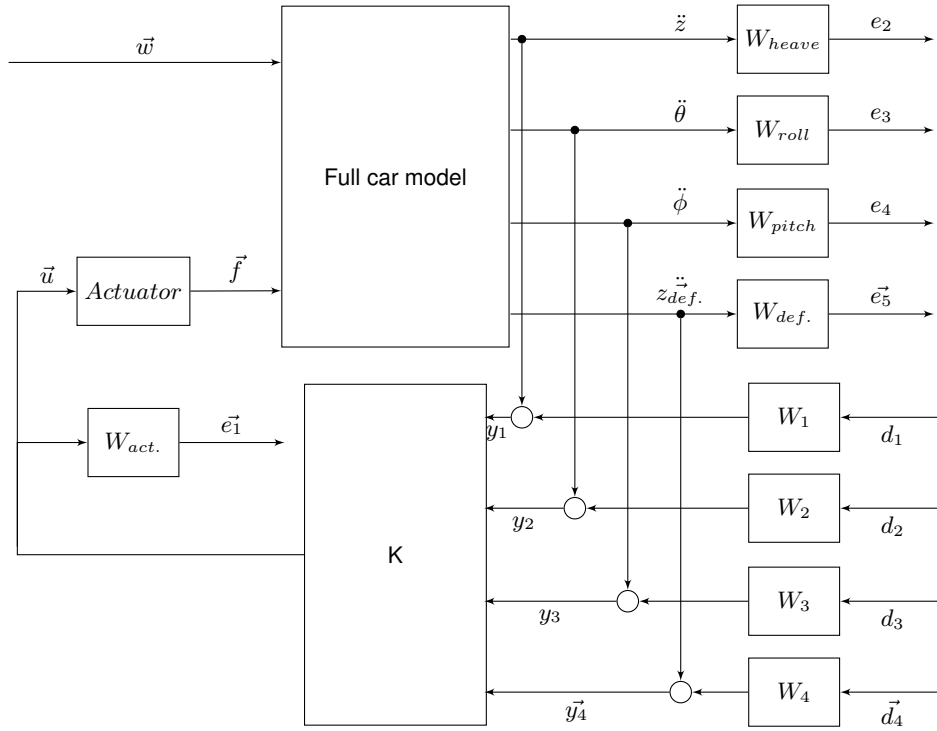
$$\|T_{ew}(s)\|_\infty = \max \bar{\sigma}(T_{ew}(jw)) \leq \gamma \quad (2.55)$$

where

$$T_{ew}(s) = P_{12}K(s)(I - P_{22}(s)K(s))^{-1}P_{21}(s) + P_{11}(s) \quad (2.56)$$

is the closed-loop transfer matrix from w to e and $\sigma(T_{ew}(jw))$ is the maximal singular value of $T_{ew}(jw)$.

The closed-loop of the active suspension with H_∞ control is shown in Fig. 2.12.

Figure 2.12.: Closed loop of H_∞ control.

where $\vec{w} = [r_1, r_2, r_3, r_4]^T$ is the input of the road signals from four wheels.

Block *Act.* represents the hydraulic actuator used for active suspension control is connected between the body mass and the wheel assembly mass. The nominal actuator dynamics are represented by the first-order transfer function. This nominal model only approximates the physical actuator dynamics. [26] use a family of actuator models to account for modeling errors and variability in the actuator. This family consists of a nominal model with a frequency-dependent amount of uncertainty.

The main control objectives are formulated in terms of passenger comfort which relates to body acceleration \ddot{z} , roll acceleration $\ddot{\phi}$, pitch acceleration $\ddot{\theta}$ and road handling which relates to the suspension deflections $\vec{z_{def.}} = [z_{def.1}, z_{def.2}, z_{def.3}, z_{def.4}]^T$, where $z_{def.i} = z_{si} - z_{wi}$.

Other factors that influence the control design include the characteristics of the road disturbance, the quality of the sensor measurements for feedback and the characteristics of the available control force actuator. In general, some weights are considered on the controlled outputs including the actuator force. They represent the performance specifications in the frequency-domain.

There are sensor noises modeled as normalized signals d_1, d_2, d_3, d_4 shaped by weighting functions

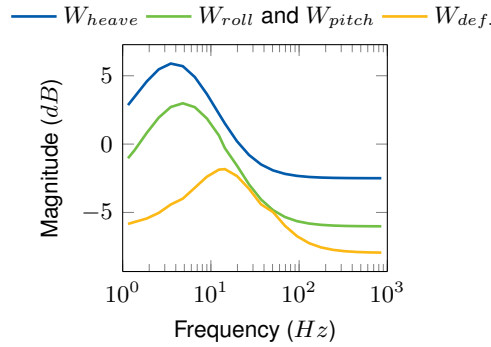


Figure 2.13.: Bode plot of weighting functions W_{heave} , W_{roll} , W_{pitch} and $W_{def.}$.

W_1, W_2, W_3, W_4 respectively on the measurements as the external sources of disturbances. In a realistic design, these weights would be frequency dependent to model the noise spectrum of the displacement and acceleration sensors.

The feedback controller uses measurements of body accelerations and suspension deflections to compute the control signal \vec{u} driving the hydraulic actuator.

Besides the inputs, outputs and feedback, the weighting functions W_{heave} , W_{roll} , W_{pitch} and $W_{def.}$ are the weight on the outputs of the FCM, which are determined according to the performance specifications and chosen to improve the transfer functions only in some frequency ranges. Because performances in high frequencies are not looked for, the transfer functions from road to vertical acceleration \ddot{z} , $\ddot{\phi}$ and $\ddot{\theta}$ are particularly weighted between $1Hz$ and $20Hz$. The transfer functions from road to suspension deflections $z_{def.}$ is particularly weighted between $8Hz$ and $30Hz$. The chosen weighting functions are described below in more details, and presented in Fig. 2.13.

The control input \vec{u} is weighted beyond $30 Hz$ according to the actuator limitations in high frequencies.

In the last, the controlled outputs are

$$e = [e_{Act.}, e_{heave}, e_{roll}, e_{pitch}, e_{def.}]^T \quad (2.57)$$

With the appropriate weighting functions of the feedback and connection of the signals the controller K can be calculated in MATLAB. The responses of the heaving, pitching and rolling motion of the vehicle body and the bode plot of the transfer functions of \ddot{z}/u_{heave} , $\ddot{\theta}/u_{pitch}$ and $\ddot{\phi}/u_{roll}$ of the FCM with active suspension in comparing with the FCM with passive suspension are shown in Fig. 2.14.

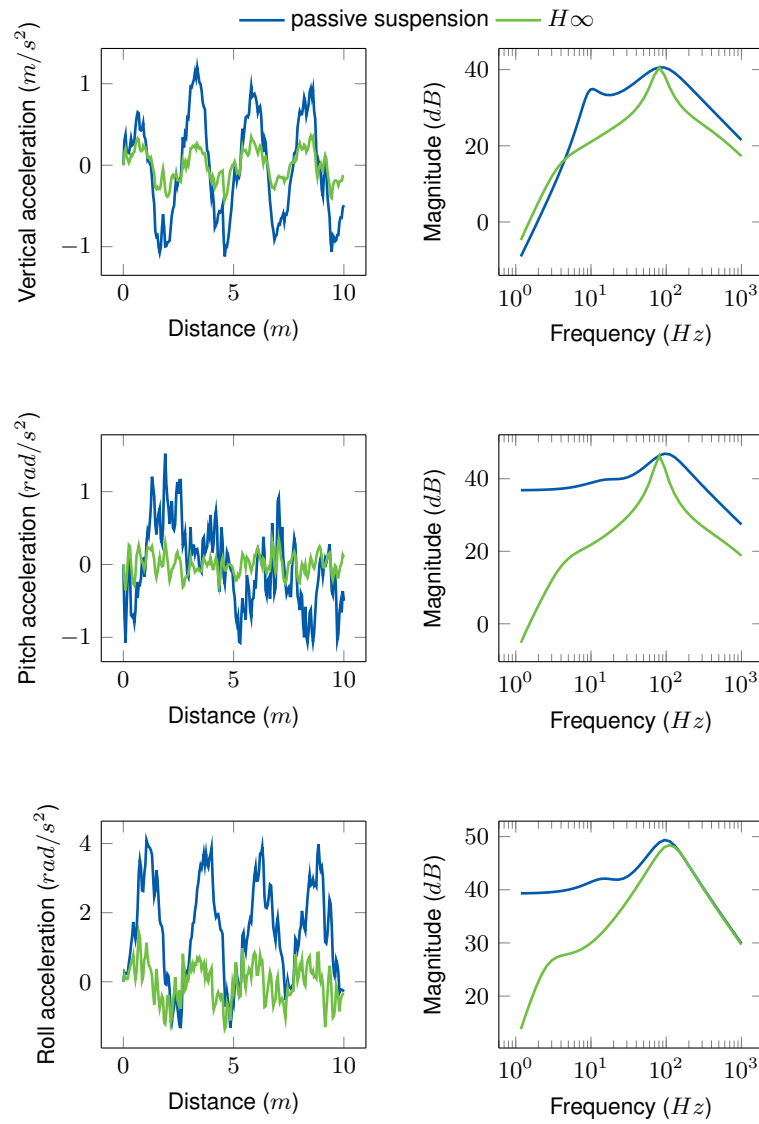


Figure 2.14.: Influence of the active suspension on the vehicle dynamics.

2.6. Position of output

According to [45] the position of output has a direct influence on the value of the vehicle body acceleration. It indicates that the collected data varies with the install position of the sensors. To find at which point of the output fills the data processing best, different positions of the outputs should be implemented.

Assume the coordinate of the output in the original coordinate system which is set in Sec. 2.2 is (a, b, c) . The general rotation can be obtained from the multiplication of the two basic rotation matrices R_x and R_y by the roll angle ϕ and pitch angle θ . The angles are right-handed and so small that the rotation matrix R is

$$\begin{aligned} R(\phi, \theta) = R_x(\phi)R_y(\theta) &= \begin{bmatrix} 1 & 0 & 0 \\ 0 & \cos\phi & -\sin\phi \\ 0 & \sin\phi & \cos\phi \end{bmatrix} \begin{bmatrix} \cos\theta & 0 & \sin\theta \\ 0 & 1 & 0 \\ -\sin\theta & 0 & \cos\theta \end{bmatrix} \\ &= \begin{bmatrix} 1 & 0 & \theta \\ 0 & 1 & -\phi \\ -\theta & \phi & 1 \end{bmatrix}. \end{aligned} \quad (2.58)$$

After rotation the new coordinate of the output is

$$\begin{bmatrix} a' \\ b' \\ c' \end{bmatrix} = \begin{bmatrix} 1 & 0 & \theta \\ 0 & 1 & -\phi \\ -\theta & \phi & 1 \end{bmatrix} \begin{bmatrix} a \\ b \\ c \end{bmatrix} = \begin{bmatrix} a + \theta \cdot c \\ b - \phi \cdot c \\ -\ddot{\theta} \cdot a + \ddot{\phi} \cdot b + c \end{bmatrix}. \quad (2.59)$$

The acceleration \vec{a}_{op} at the point of output is

$$\ddot{\vec{a}}_{op} = \begin{bmatrix} a_{opx} \\ a_{opy} \\ a_{opz} \end{bmatrix} = \begin{bmatrix} \ddot{\theta} \cdot c \\ -\ddot{\phi} \cdot c \\ -\ddot{\theta} \cdot a + \ddot{\phi} \cdot b \end{bmatrix}. \quad (2.60)$$

It is seen that when c is not zero, there are additional lateral and longitudinal acceleration at point of output. The relation between vertical acceleration of output a' and the acceleration at the center of the gravity a_z is

$$a' = a_z + a_{opz} = \ddot{z} - \ddot{\theta} \cdot a + \ddot{\phi} \cdot b. \quad (2.61)$$

Table 2.3.: Position of outputs.

$[m]$	S1	S2	S3	S4
a	0	1.345	0	1.345
b	0	0	0.856	0.856

The vehicle body is regarded as a rigid body, hence the angle motion is shared among the entire rigid body.

$$\ddot{\theta}' = \ddot{\theta}, \quad (2.62)$$

$$\ddot{\phi}' = \ddot{\phi}. \quad (2.63)$$

With equations 2.61 the output of any position (a, b, c) in the vehicle coordinate system can be derived.

Here four different positions which is labeled by S_1, S_2, S_3, S_4 are set to analysis the the influence on the outputs. The coordinate of those outputs are shown in Table 2.3. Fig. 2.6 indicates the difference of the acceleration response at different position of the vehicle in time domain and frequency domain.

Obviously the output of S2 which is at the middle of the axle of the vehicle has the minimal amplitude while the output at S4 which represents the corner of the vehicle has the maximal amplitude. Besides the amplitude, the direction of the vertical acceleration also varies with the position of the output. However, it is opposite in the frequency analysis. After the Fourier transformation the output of S2 is different from others and delivers the most information from $0Hz$ to $5Hz$. The diversity of the output signal gives the processing of the classification more options and possibilities.

2.7. Tire model

The widely used tire model for the full car simulation is the single point contact model. The tire mass is concentrated at the wheel rim and the interaction between the tire and ground is regarded as single point contact follower. The model can describe the tire's vertical force generated by the road surface correctly in most situations.

However, there is no mechanism to emulate contact patch envelopment, consequently, the point contact model does not mitigate peak vertical forces. Moreover, there is no mechanism to emulate obstacle wavelength filtering that is inherent in normal tires. when facing a shorter wavelength of the obstacles and the tire envelopes the obstacle within the contact patch, the simulated tire spindle

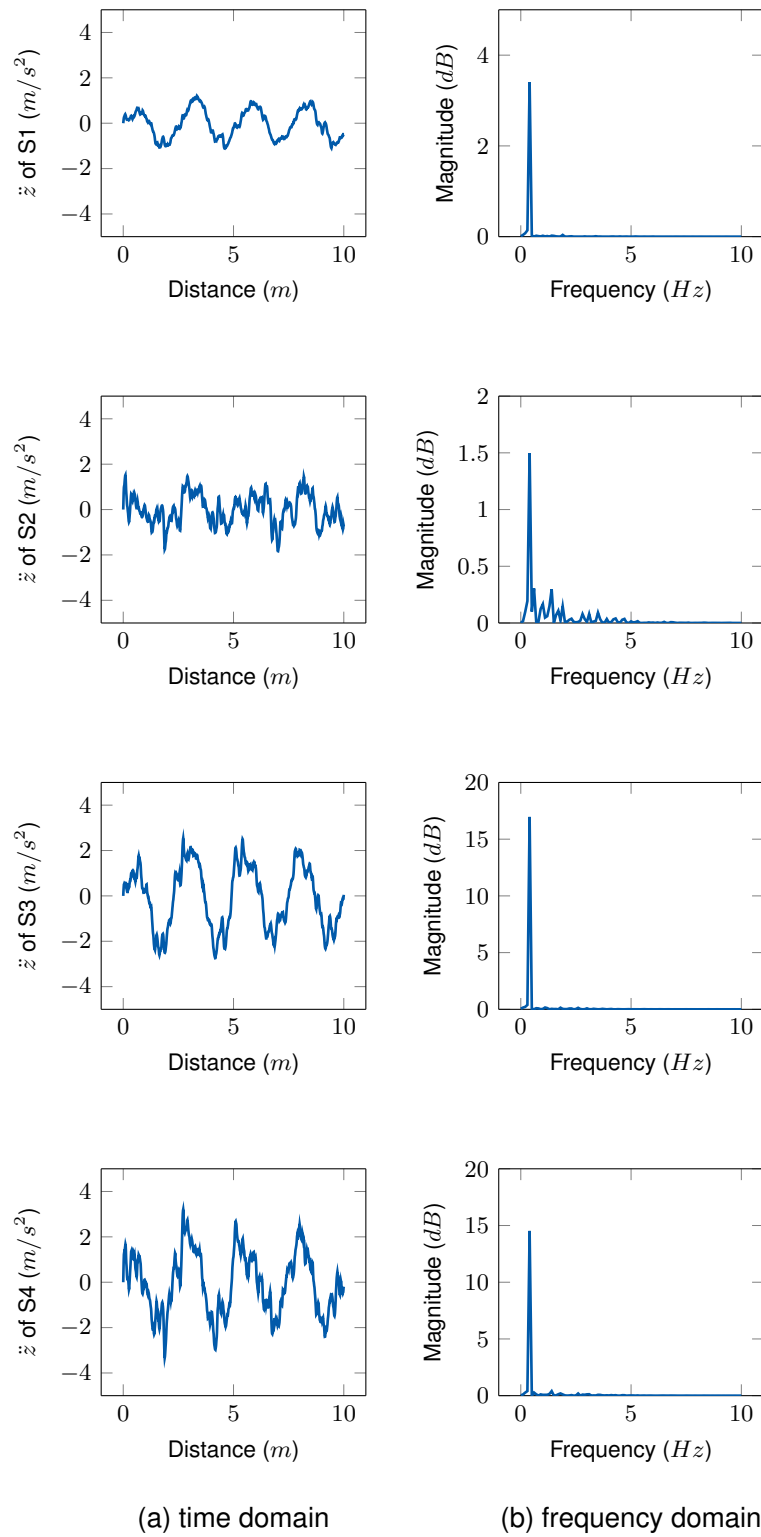


Figure 2.15.: Body acceleration at different positions of the vehicle body.

Table 2.4.: Ride phase tire model ranking via vertical acceleration [15].

obstacle wavelength less than tire contact patch length			
Tire Model	Chasis acceleration \ddot{z}	Error [%]	Ranking
Point Contact	147		4
Ring Contact	172		5
Constant Footprint	66		3
Adaptive Footprint	20		2
Rigid Ring	13		1

forces occur over a shorter time period and a greater peak than the measured forces. Thus, The point contact models is only useful for simple ride comfort modeling, should only be used judiciously and with long wavelength obstacles [15].

There are different road obstacles such as pothole, manhole and railway crossing, which have special profiles and most of the wavelengths are shorter than the tire contact patch. The simulated acceleration may be exaggerated due to the overrated vertical force by the single point contact model. Besides single pointer contact model, rigid ring tire model, footprint tire model and FTire model etc. are compared in [15]. It points out that except the FTire model is provided the best accuracy of all the tire models. However, other simpler models may be appropriate as they are less costly in terms of both testing requirements to obtain the model parameters and simulation time. Therefore, the model objective metrics need to be analyzed to determine which model will be most suitable for the ride comfort simulation task.

Tab. 2.4 indicates that rigid ring model provides the highest performance in comparison to the FTire standard when the obstacle wavelength is less than the contact patch length. Besides, it remains robust for the simulation of vertical spindle force based on a quarter cal model traversing obstacles. Hence, the rigid ring model is chosen as the tire model for the simulation.

2.7.1. Rigid Ring Model

The rigid ring model consists of a rigid ring, a rim, and a multi-point contact patch model that accounts for the tire's enveloping properties. In this model, the tire belt is modelled as a rigid ring, which is connected to the wheel rim by springs and dampers in the vertical, longitudinal and torsional directions (z, x, ω) . The rim is assumed to be fest connected to the axles. The damping ratios are assumed to be constant here. The model is shown in Fig. 2.16.

The equations of motion for the rigid ring are

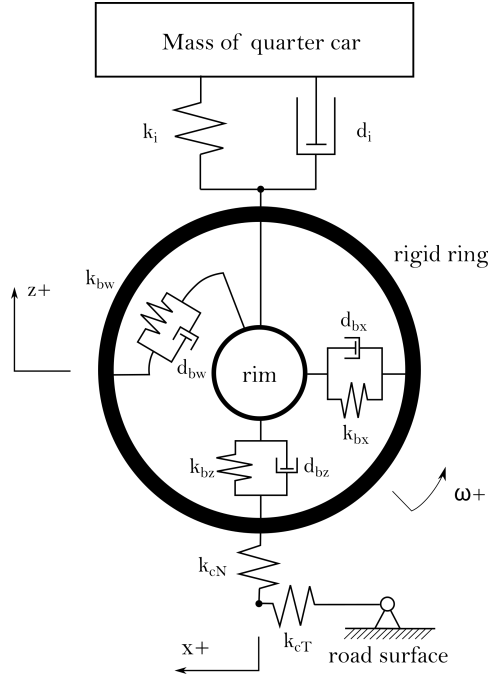


Figure 2.16.: Rigid ring model.

$$m_b \ddot{x}_b + k_{bx}(x_b - x_r) + d_{bx}(\dot{x}_b - \dot{x}_r) = \cos\beta F_{cT} - \sin\beta F_{cN} \quad (2.64)$$

$$m_b \ddot{z}_b + k_{bz}(z_b - z_r) + d_{bz}(\dot{z}_b - \dot{z}_r) = -\sin\beta F_{cT} - \cos\beta F_{cN} \quad (2.65)$$

$$I_{by} \ddot{\omega}_b + k_{b\omega}(\omega_b - \omega_r) + d_{b\omega}(\dot{\omega}_b - \dot{\omega}_r) = -r_e F_{cT} \quad (2.66)$$

where k is the stiffness coefficient, d is the damping coefficient, F_c is the force from the contact patch, which F_{cN} is the normal component and ω is the effective road surface angle, and r_e is the tire loaded radius. The subscript 'r', 'b' and 'c' indicates the component rim, rigid ring and the contact patch). The mass of the three components is denoted by m , the moment of inertia by I_y .

To implement the rigid ring tire model to the car model, we still need to build a force model for the F_c . The normal force is the combination of the normal forces between the ground surface and the tread block due to the static quarter weight of the vehicle and the spring displacement and velocity damping between the ring and the tread block normal to the effective ground plane [29]. If the stiffness coefficient of the contact patch k_{cN} and k_{cT} are already known or can be measured. The force F_c is as

$$F_{cN} = k_{cN}(x_r - x_c)\sin\beta + k_{cN}(z_r - z_c)\cos\beta + Mg\cos\beta \quad (2.67)$$

$$F_{cT} = k_{cT}(x_r - x_c)\cos\beta + k_{cT}(z_r - z_c)\sin\beta \quad (2.68)$$

If the stiffness coefficient of the contact patch is unknown or hard to measure. [48] introduces a way to describe the force of the contact patch, in which a residual deflection ρ_{zr} is used to achieve a realistic overall tire stiffness. The vertical force of the contact patch is resulted as

$$F_{cz} = q_{Fzr3}\rho_{zr}^3 + q_{Fzr2}\rho_{zr}^2 + q_{Fzr1}\rho_{zr} + q_{V1}\Omega^2 \quad (2.69)$$

where q indicate the coefficients set in cite and Ω is the rim rotational velocity. The residual deflection is as

$$\rho_{zr} = r - z_b + q_{V1}\Omega^2 \quad (2.70)$$

where w is the effective road surface height. The longitudinal force of the contace patch can be derived from the empirical Pacejka model.

$$F_{cx} = A\sin(\text{Barctan}(Cs_x)) \quad (2.71)$$

where parameter A, B, C have no direct physical meaing and are set from the system identification. s_l is the slip of the tire in the longitudinal direction and can be represented as

$$s_x = \frac{\dot{x}_b - r_e(\Omega + \dot{\theta}_b)}{\dot{x}_b} \quad (2.72)$$

Replacing the $m_u\dot{i}$ as m_r in the FCM in Sec. 2.5, then add the equation 2.64 of the rigid ring and the force model of the contact patch which is introduced in Equ. 2.67 or in cite, the rigid ring tire model is implemented in the FCM. It can be seen that in the rigid ring model the motion in the longitudinal direction is took into consideration, which is the advantage with the point contact tire model.

Besides, a more detailed and accuracy rigid ring model which is attended with a two or five point follower is introduced in [29].

2.7.2. Modified Point Contact Tire Model

The rigid ring tire model is simple and efficient, but one additional consideration for developing the improved model is its suitability for using standard laboratory tests to measure the required lumped parameters for vertical, longitudinal, and torsional sidewall stiffness as well as tread, rigid ring, and bead/sidewall mass elements of four tires [29].

Because the test laboratory is not available in the thesis, a modified point contact model is proposed to compromise the accuracy of the model and the financial situation.

The gain K is introduced to tune that is described as a function of the ratio e and the velocity of the vehicle v .

$$K = \begin{cases} a_0 + a_1 \cdot e^{a_2} \cdot v^{a_3} & (e < 1) \\ 1 & (e \geq 1) \end{cases} \quad (2.73)$$

where

$$e = \frac{l_{obstacle}}{l_{contactpatch}} \quad (2.74)$$

is the ratio between the length of obstacles and the tire contact patch. a_0, a_1, a_2, a_3 are the factors of the description of the gain K .

When the tire crosses a obstacle, whose profile is below the road surface and its length is smaller than the tire contact patch, e.g a small and deep pothole or railway crossing, the height of the obstacle will be decreased in some degree by the gain. The reason is that in this situation the real displacement of the wheel rim due to the elasticity of the rubber cannot be the same as the depth of the obstacles.

The situation is represented in Fig. 2.17. The real displacement of the wheel rim Δz_u is smaller than the irregularity of the road profile Δr . The less the ratio e which represents a shorter obstacle wavelength, the slighter the influence from the obstacle on the displacement of the wheel rim.

While the tires crosses the obstacle whose profile is above the road surface and is steep, e.g a cleat or a step, the amplitude of the signal will be increased by K . Except the vertical component of the velocity which will give an additional velocity to the wheel rim in vertical direction, the force that is generated during the crash by the obstacle has also a impact on the vehicle. The strength of

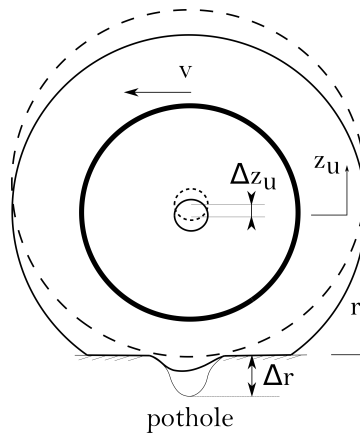


Figure 2.17.: Contact situation with a short pothole.

the impact is related to the velocity of the vehicle. The faster the velocity of the vehicle crosses the obstacle, the stronger the vibration is generated from the obstacle on the vehicle.

With this method the motion in the longitudinal direction and the interaction of the tire and the road have been considered in a simplified way. The parameters a_0 , a_1 , a_2 , a_3 will be identified in Sections 3.

3. Identification and validation

The model verification addresses the question whether the implemented model as a whole and its components conceptionally meet its criteria. According to the aim of the simulation that is to model the reality as perfect as possible, a real scenario in the simulation environment is exactly reproduced, including the elimination of errors in the model and the fine tuning of the parameters that were not available in the literature or through measurements. Considering the manufacturing and measurement tolerances, the model and the simulation will never be exactly the same. The claim for the simulation should thus be the qualitatively correct depiction of the trend shown by the real measurement.

Here the validation consist of two parts: Firstly, the identification of the damping coefficient and validation of the time response while traversing the speed bump with different velocities. Secondly, the identification of the parameters for formula 2.7.2 and validation of the vehicle vibration while traversing different obstacles with different velocities. The real measurements are performed with a BMW 116d.

3.1. Identification and validation of the damping ratio

In one of the real measurements the vehicle drives at the speed of 20km/h across a speed bump which is 13mm high and 70mm wide on only one side of the road and the sensor is in the glove compartment (S4 in Sec. 2.6). According to the principle of the validation, the situation should be identically reproduced in the simulation. The FCM which will be used in the validation is with the basic point contact tire model because the parameter in 2.7.2 is till unknown. As what is mentioned in Sec. 2.7, the point contact tire model performs good only when the wavelength of the obstacle greater than the contact patch, which is about 150mm long.

Fig. 3.1 shows the geometric relationship when the tire just meets the speed bump. It can be seen that the tire has already touched the speed bump before the vehicle arrives the start point of it (C). Hence in the simulation the start point of the speed bump should be at D , not C . On the basis of the trigonometric function it is known that

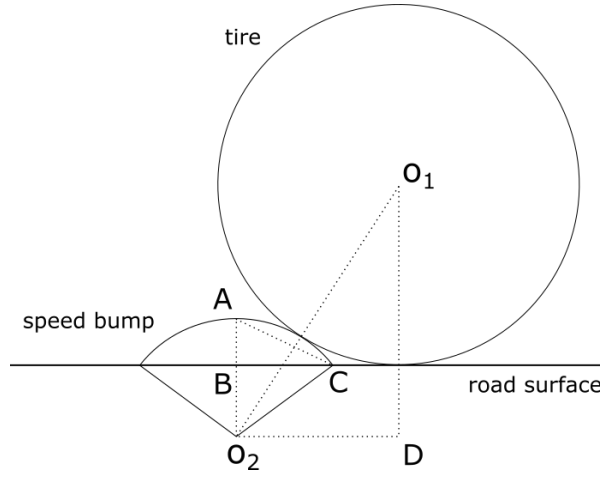


Figure 3.1.: Geometric of the tire and speed bump.

$$|AC| = \sqrt{|AB|^2 + |BC|^2} = \sqrt{13^2 + (70/2)^2} mm = 37.4 mm \quad (3.1)$$

$$\angle A = \arctan\left(\frac{|BC|}{|AB|}\right) = 70^\circ \quad (3.2)$$

$$\angle O_2 = \pi - 2 * \angle A = 40^\circ \quad (3.3)$$

With the law of sines,

$$\frac{|AC|}{\angle O_2} = \frac{r_2}{\angle A} \quad (3.4)$$

Thus $r_2 = 53.6 mm$.

The radius of tire r_1 can be read from the sidewall of the tire. From the last dimension listed in the size number '195/55R16' it is known that the diameter of the wheel rim is 16 inch. According to [44] the diameter of the tire r_1 is about 660mm.

It is easy to calculate the length $|O_2D| \doteq 100 mm$. Hence the complete length of the speed bump in the simulation should be $2 \cdot |O_2D| = 200 mm$, which is greater than the contact patch. It means the use of the basic point contact tire model is feasible in this situation.

The speed bump is modeled by a sine function which is shown in Fig. 3.1. Addition to the roughness of the asphalt surface ($IRI = 1$), the road model is created. Tuning the damping ratio of the suspensions to get the results that is most similar to the actual measurement, including the peak of the amplitude and the duration of the vibration.

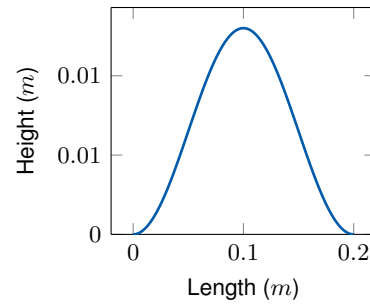


Figure 3.2.: Profile of the simulated speed bump.

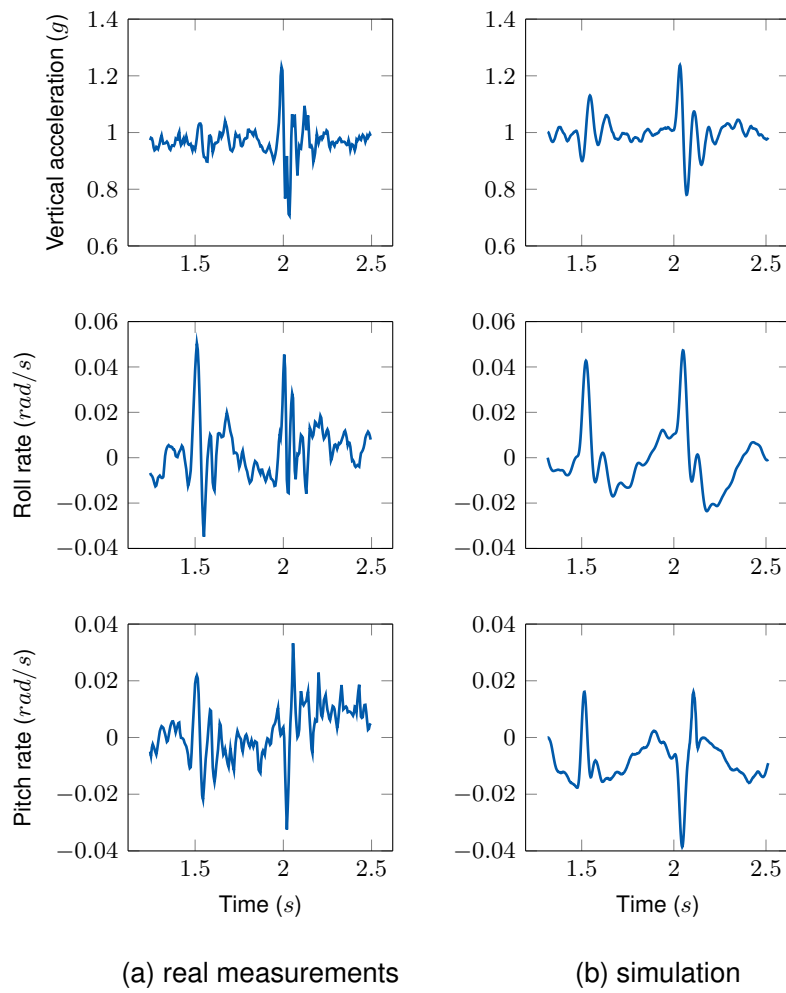


Figure 3.3.: Comparison of the vehicle response to a speed bump.

Table 3.1.: Stiffness and damping ratio of the full car model.

variable	k_1	k_2	k_3	k_4	d_1	d_2	d_3	d_4
unit	$[kN \cdot m^{-1}]$				$[kN \cdot s \cdot m^{-1}]$			
value	16	16	16	16	1	1	1	1

Table 3.2.: Parameters for K and size of different events.

events	a_0	a_1	a_2	a_3	$l/[m]$	$h/[m]$
pothole	0	0.03	1	1	0.5	0.02
manhole cover	0	0.015	0	1	0.5	0.01
cobbled road	0	0.04	1	1	0.2	0.02
railway crossing	0.02	0	0	0	1.45	0.1

The identified coefficient of the damping is shown in table 3.1. With those coefficient the comparison between the measured data and the simulation is shown in Fig. 3.1. It can be seen that although the value of the peaks do not complete match the reality, the general behaviour of the simulation is very similar to the actual measurement, which validates that the FCM can correctly simulate the behaviour of a real vehicle.

3.2. Identification and validation of the tire model

To identify the parameter in the formula 2.7.2, different obstacles with different wavelength should be tested. In the real driving test the the BMW 116d crosses six different events including asphalt road, pothole, manhole cover, railway crossing, cobbled road and evenness at four different velocities from $20km/h$ to $60km/h$

All of the following outputs are measured at the center of gravity. For each velocity and each measuring event four runs are conducted and then the averaged value of the parameter is reported. The error bars show the standard deviation of the obtained values.

The best situation is that the modified point contact model can be applied in all different obstacles after the identification. However, it hard to fulfill due to the simply structure an principle of the model. The dynamic process between the obstacle and tire is so complicated that it is difficult to build a accuracy model with the point contact model an only two variables e and v .

Thus, for different obstacles different parameters of formula 2.7.2 should be identified separately to describe the real motion of the tire and the road. Although the amount of the labor has increased,

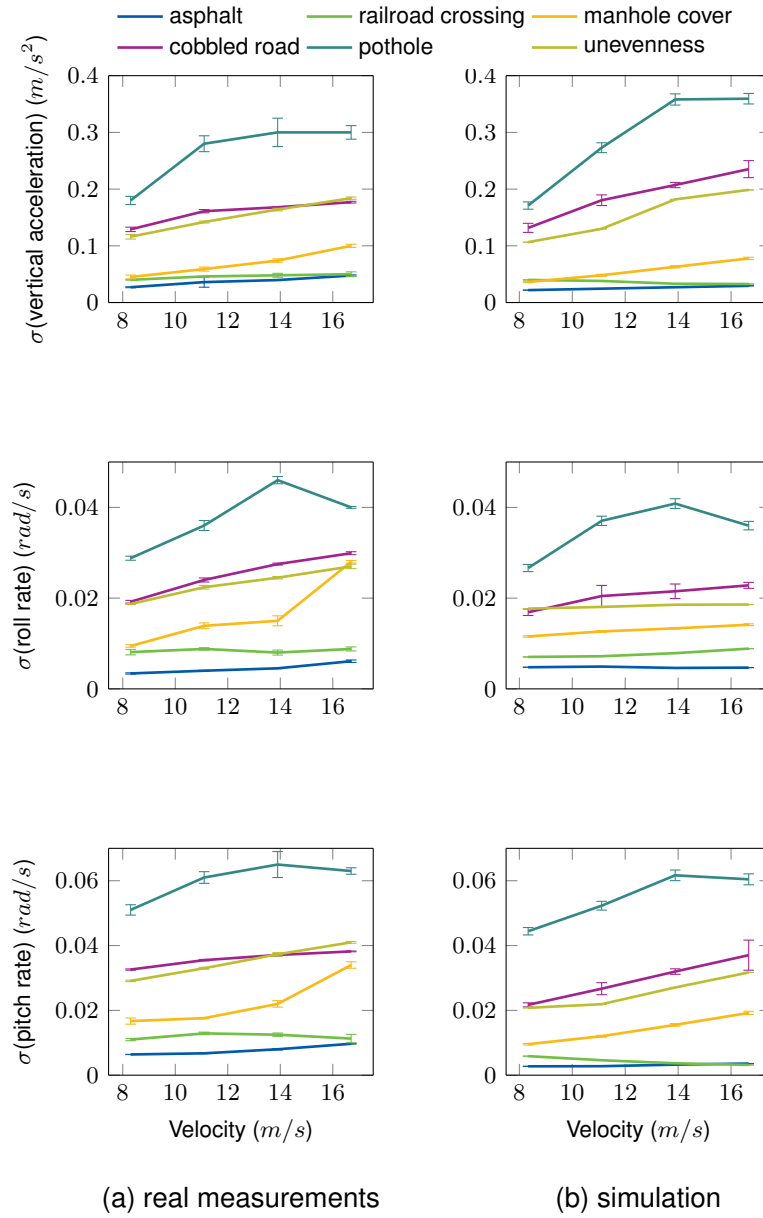


Figure 3.4.: Comparison of the standard deviation σ of vertical acceleration, roll rate and pitch rate between real measurement and simulated results.

the results proves to be satisfied. The result of the measured data and the simulation after the identification are shown in Fig. 3.2. And the identified parameters of the filter are shown in table 3.2.

It is observed that the simulated results have a very similar distribution as the measured data. Despite some simulated value has a deviation from the real data, the tendency and the relative position of different outputs by different obstacles are in general the same as the results of the measurement. These clearly and correctly divided data has a positive influence on the accuracy of the classification.

After the vehicle model and road model have been appropriately identified, the outputs provides not only a generally accuracy of the value e.g. the vertical acceleration, roll rate and pitch rate, also performs a similar features and relations compared with the actual data e.g. the duration of the signal and the standard deviations of different signals.

In conclusion, the data which has been simulated by the road- and vehicle model is proved to be in the line with the facts. Thus, the results and accuracy of the data processing in the next chapters shall be reasonable and well-founded.

4. Methodology

4.1. Data processing

The goal is to find a function f_X , which classifies the road infrastructure, e.g. the road condition, based on the vehicle dynamic data from the simulation. A supervised learning approach and a support vector machine (SVM) is used to find such a function. SVM is a supervised learning technique that can only be used for classification and regression tasks. The biggest advantage of a SVM is that it is the only technique that is explicitly based on learning theory. Other techniques like neuronal networks and decision trees have local minima as problems, which the SVM does not have, as it always tries to separate the data points with maximum margin and hence always finds the global minimum. A basic SVM is a binary, linear classifier, meaning it can only distinguish between two different classes that are linearly separable. For the use in problems that can not be separated with a straight line, the kernel-trick is applied to map the data points in a higher dimensional space where they can again be separated by a line.

It is often used for problems with a high number of features, as its performance is not affected by the number of features. Features are extracted from the raw data to reduce the dimension and to characterize the vehicle response due to various road obstacles and builds derived values intended to be informative and non-redundant. Besides, each feature set must be labeled with the ground truth data, otherwise the features are meaningless.

Determining a subset of the initial features is called feature selection. The selected features are expected to contain the relevant information from the input data, so that the desired task can be performed by using this reduced representation instead of the complete initial data [4]. The central premise when using a feature selection technique is that the data contains many features that are either redundant or irrelevant, and can thus be removed without incurring much loss of information [6]. Redundant or irrelevant features are two distinct notions, since one relevant feature may be redundant in the presence of another relevant feature with which it is strongly correlated. This results in a n -dimensional feature vector, which dimension can be reduced with feature selection and feature aggregation [16]. With statistical methods, redundant or irrelevant features can be

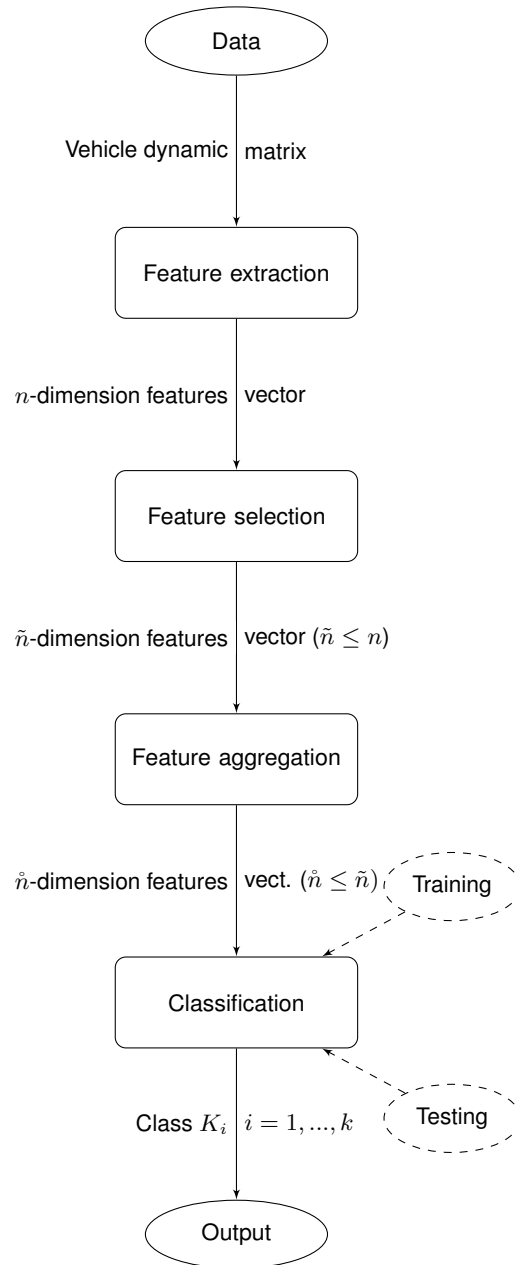


Figure 4.1.: Overview of the method to predict road features of class K_i based on vehicle dynamic data from simulation.

eliminated, which enhances the generalization and avoids over-fitting. In this thesis multivariate analysis of variance (MANOVA) is used to select the best features.

The dimension of the feature vector can be further reduced through feature aggregation. For this purpose linear discriminant analysis (LDA) is applied. After the classifier is trained, the model can be tested with new labeled data. Figure 4.1 summarizes the methods to process the vehicle dynamic data.

From the correct and false predicted instances, we can calculate a confusion matrix $M = (m_{ij}) \in \mathbb{N}^{k \times k}$ for classes $K_i, i = 1, \dots, k$. In the confusion matrix, m_{ii} presents the *true positives* for class i . The other elements in column j are called *false negatives*, in row i *false positives* and in the diagonal *true negatives*.

From the confusion matrix, one can calculate multiple performance measures to evaluate the model, such as recall with $\frac{m_{ii}}{\sum_{j=1}^n m_{ji}}$ for class K_i , the overall accuracy of the classifier with $\frac{\sum_{i=1}^n m_{ii}}{\sum_{i=1}^n \sum_{j=1}^n m_{ij}}$, or the precision $\frac{m_{ij}}{\sum_{j=1}^n m_{ij}} = \pi_{ij}$. The precision presents the fraction of retrieved instances that are relevant and can be seen as the probability π_{ij} of the classifier to predict class i as class j for $i, j = 1, \dots, l$. An overview for performance measures for different calculation problems can be found in [41]. The data is processed with the SCIXMINER toolbox for MATLAB [28].

4.2. Road events and data labelling

The Data which is used for the training and testing for the classifier is simulated by the different road model and vehicle model which is introduced in chapter 2. There are six classes of the events including asphalt road, pothole, manhole cover, railway crossing and unevenness road used in the simulation. Each of the events represents a type of obstacle is labeled from 1 to 6 as the output variables for the classification of training and as the ground truths in the process of testing. The length and height of the events can be randomly varied from 0.5 to 2.5 times over the road profile. This road model is described in Sec. 2.1. For training and testing several road profiles with multiple road events are created as the input variables of the simulation. Particularly, the profiles of the road model for testing are randomly created to investigate the robustness of the classifier which is trained by a fixed road model with a amount of variations.

4.3. Feature extraction

With the road model as the input of the full car model we can get the response outputs including vertical acceleration, roll acceleration and pitch acceleration of the vehicle body in time or space domain. The advantage of the space domain over the time domain is that every event is located at the same spot no matter how fast the car is driving, which makes it convenient and efficient to divide the windows of the data. Furthermore, the vehicle vibration is dependent on the velocity, which can be minimized by transforming the time series data into space series data [46].

The features should carry the representative information of the current road segment and be able to distinguish the difference of the response of each event. All the 98 extracted features are calculated in a certain window length of $5m$ and overlap 50% from the whole response outputs. The features include the mean velocity of the vehicle; maximum, minimum and mean value of the signals; range between the maximum and minimum; duration between the two extreme, root mean square (RMS) which is defined as the square root of the mean square, and standard deviation (Std). These features can reflect the character of the data in the space domain.

As well as integration of the band-pass filter for a certain frequency range (intBP) from $1Hz$ to $30Hz$ with the interval $2Hz$ which indicates the weight of the selected frequency in all the pass band, maximum of the band-pass filter for a certain frequency range (maxBP) from $1Hz$ to $30Hz$ with the interval $2Hz$ which indicates the maximum magnitude of the selected frequency, power spectral density (PSD) which describes the distribution of power into frequency components, and the spectral centroid which indicates where the 'center of mass' of the spectrum is and hence represents the the most common frequency in this window. These features can reflect the character of the data in the frequency domain.

4.4. Display and evaluation of the classification

The results will be evaluated in this chapter by the confusion matrix and graphics. In the display of the graphic the axes represent the selected features, the color of the point cloud represents different events. The clouds may be overlapped or separated, which represent the performance of the classifier with those selected features.

In the confusion matrix each class has one row and one column in this matrix and they are arranged in the same order. The rows represent the actual class membership and columns represent the predicted class. This means that all correctly classified data points are the diagonal elements of the

Table 4.1.: Example of a confusion matrix

		Prediction	
		+	-
Actual class	+	true positive	false negative
	-	false positive	true negative

matrix. While other points are classified false. An example of a confusion matrix is presented in table 4.1.

There are three performance measures to get meaningful information from the confusion matrix. The first measure is 'Precision'. This measure represents for each class the percentage of correctly classified members of this class among all points that were predicted as members of this class by the classifier. Take the confusion matrix 4.1 as the example of calculation

$$Precision_+ = \frac{\Sigma true\ Positives}{\Sigma predicted\ condition\ positive} \quad (4.1)$$

The second measure is 'Recall'. It represents for each class the percentage of correctly classified members of this class among all actual members of this class.

$$Recall_+ = \frac{\Sigma true\ positives}{\Sigma total\ number\ of\ actual\ Positives} \quad (4.2)$$

The last measure is 'Accuracy'. It is a general evaluation of the performance of a classifier.

$$Accuracy = \frac{\Sigma true\ positives + \Sigma true\ negatives}{\Sigma total\ number\ of\ data\ point} \quad (4.3)$$

From these performance measures it can be seen whether the classifier performs good for all classes or only several classes.

In supervised learning applications in machine learning and statistical learning theory, generalization error is a measure of how accurately an algorithm is able to predict outcome values for previously unseen data. Because learning algorithms are evaluated on finite samples, the evaluation of a learning algorithm may be sensitive to sampling error. As a result, measurements of prediction error on the current data may not provide much information about predictive ability on new data.

The generalization error G is the difference between the expected error $I[f_n]$ and empirical error $I_S[f_n]$.

Table 4.2.: Parameter of 3 vehicles

	l [m]	b [m]	M [kg]	k [N/m]	d [N · s/m]	m_{tire} [kg]	k_{tire} [N/m]
BMW 116d	2.69	1.71	1400	160000	1000	22.5	36689/35902
BMW 116d $load_1$	2.69	1.71	1600	160000	1000	22.5	36689/35902
BMW 116d $load_2$	2.69	1.71	1800	160000	1000	22.5	36689/35902
S-Klasse W220	2.97	1.57	2000	180000	3900	22.5	61356/54908
Sprinter	3.67	1.9	2100	180000	3900	25	36300/36300

$$G = I[f_n] - I_S[f_n] \quad (4.4)$$

Generalization error can be minimized by avoiding overfitting or overtraining in the learning algorithm. In general, this error should shrink with the amount of training data before the testing.

4.5. Variation of simulation

There are many parameters influencing the classification process. Regarding the variation of the vehicles, the model and physical parameters of the vehicle, the type of suspension e.g. passive suspension, passive suspension with anti-roll bar and active suspension as well as different loads e.g. passengers and goods in the vehicle while driving all have a influence on the collected data.

How does the classifier perform when the load of the vehicle changes. Whether a classifier which is trained by one model of vehicle can be general applied on another vehicle. What if, when a classifier trained by the data of the passive suspension is used on a vehicle with active suspension. In terms of the those questions, the simulation of the classification with different vehicle models need to be executed.

The size and physical parameters of different vehicles are shown in table 4.2. The $load_1$ and $load_2$ has an additional mass of 200 kg and 400 kg on the vehicle respectively. Besides, the stiffness of the tire k_{tire} is represented as k_{front}/k_{rear} . Inclusive the length, width and mass of the chassis, it represents the difference of different models. Furthermore, the FCM with passive suspension, anti-roll bar and active suspension in 2.2 to 2.5 are implemented to test the performance of the classifier on different type of suspensions.

Not only the variation of the vehicle, different position of the outputs which is introduced in Sec. 2.6 has also a influence on the classification because the outputs can provide different amount of information in different position of the vehicle. The FCM with different position of outputs e.g. center,

axle, side and corner of the vehicle which are indicated by S1, S2, S3 and S4 respectively are implemented to find the best position of the output dependent on the accuracy of the classifier. The coordinates $(a, b, 0)$ of the four positions in the coordinate system of FCM are represented in the table 2.3.

As stated before, Other important options is the setting of the number of selected features, which is a crucial step for the classification. Processing with the same data, the accuracy of classifiers which contain different selected features will be compared to determine the best setting of the feature selection. Another important option is the order of the polynomial kernel for the SVM. This means the order of separation function, which will be calculated by the SVM. A kernel order of one results in a linear separation function in the input space and a kernel order of two in a parabolic separation function. By comparing the generalization error which measures the accuracy of the classifier to predict outcome values for previously unseen data, the influence of those variations and the best matched settings for the classification can be determined.

5. Implementation

Another feature of mechatronic systems is integrated digital information processing [19]. For this purpose some software is used to solve problems. Consequently, the work on the employed software will be explained in this chapter.

5.1. Introduction of the software

MATLAB is a numerical solution software environment for many technical and scientific problems. It's suitable for quick analysis and synthesis dynamic processes in research and industry. Meanwhile it has become the standard tool for many types of technical calculations as well as simulations in system dynamics, control engineering, aviation and vehicle developing.

MATLAB comes with a basic set of tools for visualizing data and for performing calculations on matrices and vectors. For specific technologies, it provides toolboxes, which add to the basic functionality. The toolboxes used in this work are

- Control System Toolbox™
- Signal Processing Toolbox™
- Robust Control Toolbox™
- SCIXMINER (available under <https://sourceforge.net/projects/scixminer/>)

Control System Toolbox™ provides algorithms and apps for systematically analyzing, designing, and tuning linear control systems. We can specify the system as a transfer function, state-space, zero-pole-gain, or frequency-response model and analyze, visualize the system behavior in the time and frequency domains [24].

Signal Processing Toolbox™ provides functions and apps to generate, measure, transform, filter, and visualize signals. The toolbox includes algorithms for resampling, smoothing, and synchronizing signals, designing and analyzing filters, estimating power spectra, and measuring peaks, bandwidth,

and distortion. We can use Signal Processing Toolbox to analyze and compare signals in time, frequency, and time-frequency domains, identify patterns and trends, extract features, and develop and validate custom algorithms to gain insight into the data [27].

Robust Control Toolbox™ provides functions and blocks for analyzing and tuning control systems for performance and robustness in the presence of plant uncertainty. We can analyze the impact of plant model uncertainty on control system performance, and identify worst-case combinations of uncertain elements. H-infinity and mu-synthesis techniques can maximize the robust stability and performance of the controllers [26].

5.2. Explanation of the scripts in MATLAB

Here the basic part and the used commands in the script will be explained. The version of MATLAB which is used for the thesis is 2016a. The details are hidden by abridgments due to the limit of the space.

The road model is wrote as a function which can create a road profile with the given roughness and random number of obstacles that are distributed on the random position on the road.

Listing 5.1: Function of the road model

```

1 function profile = road_model(typ)
2 ...
3 % PSD is a function for creating a random road.
4 % road is an empty matrix for storing the value of the desired
   road.
5 roughness = PSD(IRI,L);
6 road = zeros(size(roughness));
7 ...
8 % cut the road into 100 pieces for inserting obstacles
9 interval = L/100/dr;
10 % random number of the obstacles (from 5 to 20)
11 n = randi([5 20],1);
12 % random position of the n obstacles on the road
13 position = randi([1 100],[1 n]);
14 % random gain (0.5 to 2.5) for shape of the obstacle
15 k = 0.5+2*rand(2,n);
16 ...

```

```

17 for i = 1:n
18     if strcmp(typ,'pothole')
19         % a/b is the length/height of the obstacle which are
           modified by k
20         a = k(1,n)*0.3;
21         b = k(2,n)*0.05;
22         % function of the pothole
23         obstacle = pothole(a,b);
24     elseif strcmp(typ,'manhole cover')
25         ...
26     end
27     % insert the obstacle at the corresponding position
28     road(interval*(n-1)+1:interval*(n-1)+length(obstacle)) =
           obstacle;
29 end
30 % add the roughness
31 road = road + roughness;
32 ...
33 end

```

where 'typ' is the type of the obstacle including 'pothole', 'manhole_cover', 'cobbled_road', 'railway_crossing' etc. 'dr' is the sampling length of the road. 'PSD' and 'pothole' are the function of the random road which are explained in Sec. 2.1 The output 'profile' is a matrix with two rows which store the information of the road profiles under the left and right wheels separately.

The FCM is also wrote as a function. Here the road model which contains the road profiles of both side is as the input of the function. The output of the function is the desired accelerations such as \ddot{z} , $\ddot{\phi}$ and $\ddot{\theta}$ etc.

Listing 5.2: Function of the FCM

```

1 function Output = FCM_passive(road_left,road_right,V,auto)
2 ...
3 if strcmp(auto,'BMW_116d')
4     % body mass
5     Ms=1400;
6     % tire spring of front-right
7     Kwr1=160000;
8     % suspension damper of front-right

```

```

9      Csr1=1000;
10     ...
11     elseif strcmp(auto,'S-Klasse_W220')
12     ...
13     end
14     ...
15     % sampling time
16     dt = dr/V;
17     % running time of the simulation
18     tmax = L/V;
19     % time array
20     t = 0:dt:tmax;
21     % length of the car
22     car = round((Lf+Lr)/dr);
23     % front axle is one car ahead of the rear axle
24     left1 = road_left(car+1:end);
25     right1 = road_right(car+1:end);
26     left2 = road_left(1:end-car);
27     right2 = road_right(1:end-car);
28     ...
29     % to implement the dynamic system as a state space model
30     fcm = ss(A,B,C,D);
31     % input is the road profile of each wheel
32     input = [right1;left1;right2;left2];
33     % solve the system with the input in time 't'
34     output = lsim(fcm,input,t);
35     ...
36     end

```

where 'V' is the setting velocity of the vehicle. 'auto' is the model of the selected vehicle. 'A', 'B', 'C' and 'D' are the Matrices of the state space which is introduced in Sec. 2.2. The command 'ss' and 'lsim' in the Control System ToolboxTM are used to create and solve the dynamic system.

Besides the road model and FCM there are also several commands that will be used for the modelling and data processing.

To design a filter for the feature extraction in Sec. 4.3 and the weighting function in Sec. 2.5, the Butterworth filter is chosen for its flat pass bands and wide transition bands.

Listing 5.3: Butterworth filter design in Matlab

```
1 [b,a] = butter(n,Wn,ftype)
```

It designs a lowpass, highpass, bandpass, or bandstop Butterworth filter, depending on the value of 'ftype' and the number of elements of 'Wn'. The resulting bandpass and bandstop designs are of order $2n$. 'b' and 'a' are the transfer function coefficients of the filter.

To build the model of the FCM with active suspension, the command below is used in Sec. 2.5 to compute q stabilizing H_∞ optimal controller.

Listing 5.4: H_∞ controller design in Matlab

```
1 K = hinfsyn(P,NMEAS,NCON)
```

where 'K' is the desired controller. 'P' is the plant including the weighting functions. 'NMEAS' and 'NCON' are the numbers of control signals and measurement signals.

5.3. Working with SCIXMINER

SCIXMINER bases on MATLAB is designed for the visualization and analysis of time series and features with a special focus to data mining problems including classification, regression, and clustering [25]. It was developed at the Institute of Applied Computer Science of the Karlsruhe Institute of Technology.

The graphical user interface of SCIXMINER contains menu items and control elements like listboxes, checkboxes and text fields. SCIXMINER use the project file *.prjz as the import of data, which can be generated by the function generate_new_scixminer_project.

Apply the design with the appropriately setting of the features selection e.g. MANOVA, number of the features and type of classifier, the classification will be executed. This process can be also automatically completed by macros, which are files containing sequences of clicked menu items and control elements.

Listing 5.5: Marcos of the SCIXMINER

```
1
2 %% training %%
3
4 % Selection of single features
```

```
5 % {'MANOVA'}
6 set_textauswahl_listbox(gaitfindobj('
    CE_Klassifikation_Merkmalsauswahl'),{'MANOVA'});eval(
    gaitfindobj_callback('CE_Klassifikation_Merkmalsauswahl'));
7
8 % Number of selected features
9 set(gaitfindobj('CE_Anzahl_Merkmale'),'string','15');eval(
    gaitfindobj_callback('CE_Anzahl_Merkmale'));
10
11 % Chosen classifier
12 % {'Support Vector Machine'}
13 set_textauswahl_listbox(gaitfindobj('
    CE_Klassifikation_Klassifikator'),{'Support Vector Machine'});
    eval(gaitfindobj_callback('CE_Klassifikation_Klassifikator'));
14
15 % Kernel order
16 % 1
17 set(gaitfindobj('CE_SVM_Ordnung'),'string','1');eval(
    gaitfindobj_callback('CE_SVM_Ordnung'));
18
19 % Graphical evaluation of classification results
20 set(gaitfindobj('CE_Anzeige_KlassiErg'),'value',1);eval(
    gaitfindobj_callback('CE_Anzeige_KlassiErg'));
21
22 % Save confusion matrix in file
23 set(gaitfindobj('CE_Konfusion_Datei'),'value',1);eval(
    gaitfindobj_callback('CE_Konfusion_Datei'));
24
25 %% Classification, Data mining, Design and apply
26 eval(gaitfindobj_callback('MI_EMKlassi_EnAn'));
27
28 %% Data mining, File, Save classifier
29 eval(gaitfindobj_callback('MI_Classifier_Export'));
30
31
32 %% testing %%
33
```

```
34 %% Data mining, File, Load classifier
35 eval(gaitfindobj_callback('MI_Classifier_Import'));
36
37 %% Classification, Data mining, Apply
38 eval(gaitfindobj_callback('MI_EMKlassi_An'));
```

In the macro, the method of the feature selection is set as MANOVA, the number of the selected features is 15, the method of the classification is set as SVM and the order of the kernel is one.

After the processing of the data, the results will be graphical evaluated and the confusion matrix will be saved in files. Besides, the trained classifier will also be saved and be applied to the testing process.

6. Results

6.1. Variation of vehicle parameters

Here the performance of the classifiers applied in same or different vehicles will be analysed. To better compare the variation of vehicles, the setting of the classification in SCIXMINER is set to be invariant. The number of the selected feature is set to 15 and the order of the kernel is set to one. The position of the output is at the middle point of the front axle.

6.1.1. Classification accuracy

In this part the classifier is trained by the data which is simulated from the BMW 116d passive full car model driving on a $4km$ -long road with fixed size of events. The number of overdrives is approximately equally distributed over the events. The accuracy is 98.2 % on average. The confusion matrix of the training is shown in table 6.1. It can be seen that there is some missclassification among asphalt, manhole cover and railway crossing. The outliers may be caused by the similar distribution of the response signals when traversing the asphalt, manhole cover and railway crossing in the validation process, which is shown in fig. 3.2. In general, the classifier can tell the difference of these classes clearly.

Fig. 6.1.1 shows the classes in feature space, described by two aggregated features from 15 single features. The figure indicates, that the road features pothole and cobbled stones are clearly separable to the other classes. Unevenness is close to the road features railway and cobbled stones but still good divisible. However, railway crossing, manhole cover and smooth asphalt are very close and show some missclassifications. The aggregated features are good for graphic representation but difficult to interpret. The most important selected single features for this classification problem are discussed in Section 6.1.2.

The process of training and testing is also applied in other different types of vehicles and vehicle set-ups. The results are shown in Table 6.2. It is obvious that the separately trained classifiers reach a good accuracy in the testing. Overall, the generalization error remains good with a maximum

Table 6.1.: Confusion matrix of the training with BMW 116d passive suspension

true class	prediction						recall
	as.	ph.	m.c.	c.r.	r.c.	un.	
asphalt	231	0	9	0	1	0	96%
pothole	0	206	0	0	0	0	100%
manhole cover	10	0	226	10	0	0	96%
cobbled road	0	0	0	316	0	0	100%
railway crossing	2	0	0	0	234	0	99%
unevenness	0	0	0	0	0	316	100%
precision	95%	100%	96%	97%	99%	100%	98.2%

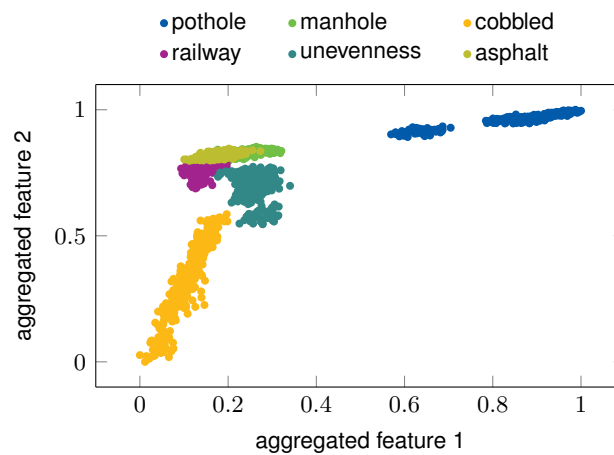


Figure 6.1.: Classes separated by two aggregated features from 15 single features.

Table 6.2.: Performance of classifiers for different vehicles.

Vehicle		Precision	Recall	Accuracy	Generalization error
BWM 116d	training	98.6 %	98.6 %	98.2 %	7.6 %
	testing	90.4 %	90.8 %	90.6 %	
BMW 116d anti-roll bar	training	99.1 %	99.3 %	99.2 %	9.1 %
	testing	88.5%	91.6%	90.1%	
BMW 116d act. susp.	training	99.4 %	100 %	99.7 %	8.5 %
	testing	90.8 %	91.6 %	91.2 %	
S-Klasse W220	training	98.2 %	97.4 %	97.8 %	10.2 %
	testing	86.1%	89.0%	87.6%	
Sprinter	training	99.9 %	99.8 %	99.9 %	5.0 %
	testing	94.9 %	94.9 %	94.9 %	

of 10.2 %. It signifies the feasibility of method using the data-mining to classify the acceleration signals.

6.1.2. Feature selection

The results of three different classifier which have been trained respectively by FCM with passive suspension, passive suspension with anti-roll bar and active suspension is shown in fig. 6.1.2. The data is classified by the best three features among the 15 features which are selected by MANOVA, which is indicated by the three axle. It is observed that the points are divided into different parts in the space, despite there are some overlaps. Those overlaps shall be separated in the classification of other features.

The most important factors of the classification in passive suspension are range of the pitch acceleration, intBP of the roll acceleration from $5Hz$ to $7Hz$ and intBP of the roll acceleration from $9Hz$ to $11Hz$. These are most important features to separate the six classes. The range of the pitch acceleration of pothole due to the greater and longer excitation in vertical direction are obviously larger than others. The intBP of the roll acceleration is the critical criterion to classify other classes because the roll acceleration of cobbled road and unevenness due to the irregular distribution are larger than that of asphalt, manhole cover and railway crossing. The length of the cobble and unevenness correspond to different frequencies of the output signals. The cobbled road with small cobbles has a greater part of intBP from $9Hz$ to $11Hz$, while unevenness with long curves has a greater part of intBP from $5Hz$ to $7Hz$.

Instead of intBP of roll acceleration, the intBP of pitch acceleration plays an important role in the

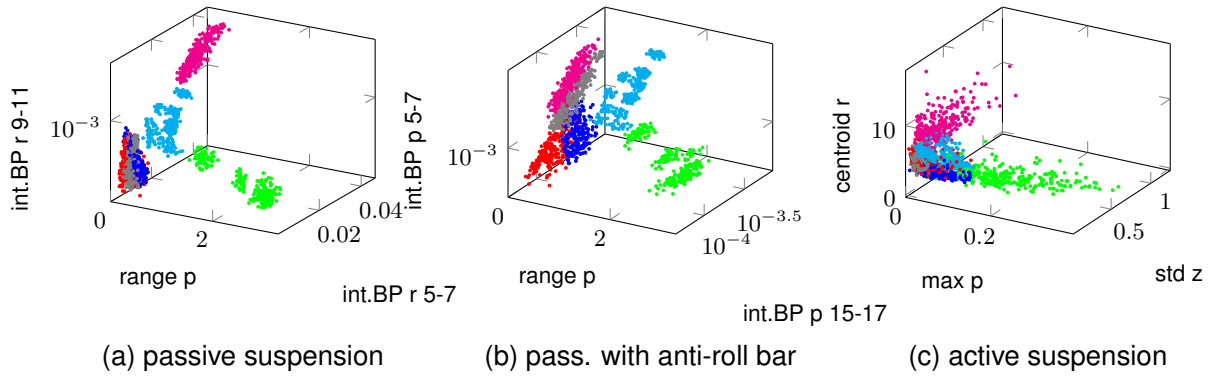


Figure 6.2.: The classification with best 3 features of different suspensions

classification while the response of the roll acceleration is significantly reduced by the anti-roll bar. The range of the pitch acceleration classifies the pothole and unevenness from others clearly. The value of the intBP from $5Hz$ to $7Hz$ of pitch acceleration is much smaller than that of roll acceleration before, which classifies the cobbled road, railway crossing, manhole cover and asphalt. Due to the wider band-pass caused by the random shape of the cobbles, the intBP of cobbled road has higher values than others. Besides, the unevenness has the most part of the intBP in high frequencies ($15Hz$ to $17Hz$).

The features of the classification with active suspension are different to the previous simulations. The response of vertical-, roll- and pitch acceleration have been reduced by the regulation of the controller. The maximum value of pitch acceleration, Std of vertical acceleration and the centroid of roll acceleration are selected as the most important features to represent the difference of classes. Moreover, the distribution of the classes is not as well as above, which indicates the difficulty of the classification for FCM with active suspension.

6.1.3. Application of the classifier

From 6.1.1 it is known that the classifier has a satisfied accuracy when it is only tested on the data of the same source. That is to say, in the application every different vehicle needs a different classifier which is specially trained for itself. It seems to be laborious and time-consuming.

Then we use the classifier which is trained by BMW 116d to predict unseen data, which are simulated by other different vehicles, loads and suspensions. In the simulation the FCM drives on a $2km$ -long road model with random size of events. The testing results are shown in table 6.3.

Table 6.3.: Performance of the classifier for BMW 116d applied on different vehicles.

Vehicle	Precision	Recall	Accuracy	Generalization error
BMW 116d 200kg loaded	87.1 %	88.3 %	87.7 %	10.5 %
BMW 116d 400kg loaded	81.2 %	80.8 %	81.0 %	17.2 %
BMW 116d anti-roll bar	82.1 %	80.7 %	81.4 %	16.8 %
BMW 116d act. susp.	42.7 %	38.0 %	40.4 %	57.8 %
S-Klasse W220	77.2 %	68.4 %	72.8 %	25.4 %
Sprinter	75.6 %	68.5 %	72.1 %	26.1 %

It can be seen when the classifier applies on the same vehicle but with different loads, the accuracy of the testing declines from 90.6% to 87.7% till 81.0% with the increasing of the load on the vehicle. This means that the classifier is not robust enough because its performance is affected by the changing load, which is very common in daily life.

When the classifier is applied on the same vehicles but with different type of suspension, the accuracy falls down especially on the active suspension. This may due to the different selected features in the respective classification. As mentioned in Sec. 6.1.2, the best features of the three different suspension and the distribution of the data in the space are not same cause the different dynamic of different suspensions.

When the classifier is applied on other vehicles, e.g. S-Klasse W220 and Sprinter, the accuracy of the classifier also declines, which means the mass, size and parameters of spring and damping all has an individual effect on the accuracy of the classifier.

With the current features it is hard to implement the classifier into other occasions. Thus except the the 98 extracted features, the load on the vehicle, the paramter of the veicle and the type of the chassis which have unignored influences on the classification should be also considered as the inputs of the data. The three variatons will be extracted as three new features: load, vehicle and suspension which represent the current load on the vehicle, the model of vehicle that is driving on the road and the suspention type of it.

To get the data of all variations, a simulation including the six different road events, loads from 0kg to 400kg, chassis with anti-roll bar, passive and active suspensions and vehicles including BWM 116d, S-Klasse W220 and Sprinter have been executed. The total length of the simulated distance is 180km and the result of the classification is shown in table 6.4.

The accuracy of the new trained classifier is 99.2%. Then apply it in all the occasions which are already tested in table 6.3. The new result of the testing is shown in table 6.5.

Table 6.4.: Confusion matrix of the training with all variations

true class	prediction						recall
	as.	ph.	m.c.	c.r.	r.c.	un.	
asphalt	6107	0	13	0	0	0	99.8%
pothole	180	2880	0	0	0	0	94.0%
manhole cover	36	0	2844	10	0	0	98.8%
cobbled road	0	0	0	4140	0	0	100%
railway crossing	0	0	0	0	3060	0	100%
unevenness	0	0	0	0	0	4140	100%
precision	96.6%	100%	99.5%	100%	100%	100%	99.2%

Table 6.5.: Testing results of the classifier of all variations

Vehicle	Precision	Recall	Accuracy	Generalization error
BMW 116d 200kg loaded	73.5 %	75.9 %	74.7 %	24.5%
BMW 116d 400kg loaded	82.2 %	79.4 %	80.8 %	18.4%
BMW 116d anti-roll bar	82.0 %	77.2 %	79.1 %	20.1%
BMW 116d act. susp.	80.4 %	78.0 %	79.2 %	20.0%
S-Klasse W220	81.4 %	74.0 %	77.7 %	21.5 %
Sprinter	73.8 %	76.2 %	75.0 %	22.2%

It can be seen that several accuracies of the classifier are probably not as good as the classifier in table 6.5, but the performance of the classifier is much robust even it is applied on different chassis and vehicles. What's more, the accuracy of the test on the active suspension is two times better than before. It shows that the performance and robustness of the classifier has improved with the additional features. Furthermore, all the results are based on the setting of 15 selected features and one order of kernel. There is still room for improvement with a better settings of the classification.

6.2. Variation of simulation

The influences of the position in the simulation is shown in Fig. 6.2. It is observed that the best accuracy can be achieved with output obtaining from position S2. Because in this position the output signal provides the most information in the frequency domain, which offers the classification more options and potentiality.

Besides the position of outputs, the number of selected features and the order of kernel have also affected the accuracy of the classification. In the practical application on the vehicle, the classifier

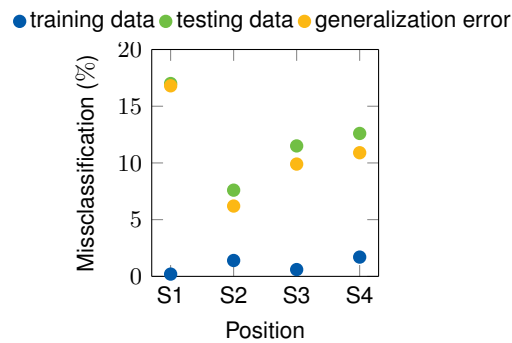


Figure 6.3.: Influence of different position on the accuracy of the classification.

Table 6.6.: Missclassification of application in BMW 116d with passive suspension

	number of selected features				
[%]	10	15	20	25	30
kernel oder	10	15	20	25	30
1	27.46	25.77	25.62	18.46	20.23
2	24.85	21.92	20.15	13.08	18.00
3	25.69	19.62	16.00	13.38	16.23
4	26.15	19.46	18.23	15.85	15.38
5	26.00	20.23	19.08	16.31	16.46

should at least maintain at a high level no matter how the load of the vehicle changes. Thus each data flow contains the output simulated by a selected vehicle model driving across different road events with a series of loads from $0kg$ to $400kg$. The number of selected features is set from 10 to 30. The order of the kernel is set from 1 to 5. Test the data with every association of those settings separately. The results are represented in the blow five tables.

The best result of all the five tables is located in the column that indicates the setting of 25 selected features. As to the setting of the kernel oder, the order two has a good accuracy which is close or even better than that of kernel order three. However, the missclassification of the vehicle with active suspension is obvious higher (17.54%) than kernel oder three (15.17%).

Table 6.7.: Missclassification of application in BMW 116d with anti-roll bar

	number of selected features				
[%]	10	15	20	25	30
kernel oder	10	15	20	25	30
1	23.00	19.77	21.31	15.62	19.38
2	21.92	18.23	17.54	13.85	17.46
3	22.77	17.62	16.62	14.38	15.92
4	23.08	18.08	16.62	16.08	16.62
5	23.31	18.54	17.72	17.23	17.15

Table 6.8.: Missclassification of application in BMW 116d with active suspension

[%]	number of selected features				
kernel oder	10	15	20	25	30
1	24.46	21.23	22.15	19.38	19.23
2	23.00	18.92	17.54	17.54	17.69
3	23.63	17.85	17.54	15.17	16.46
4	24.23	17.46	16.23	16.08	16.62
5	24.23	17.15	17.15	15.54	17.23

Table 6.9.: Missclassification of application in S-Klasse W220 with passive suspension

[%]	number of selected features				
kernel oder	10	15	20	25	30
1	23.37	23.38	23.54	15.92	15.38
2	21.54	23.38	19.77	12.37	18.62
3	25.62	22.00	18.37	12.37	18.77
4	27.62	23.08	22.69	15.23	21.15
5	28.39	25.00	24.85	14.92	24.00

Table 6.10.: Missclassification of application in Sprinter with passive suspension

[%]	number of selected features				
kernel oder	10	15	20	25	30
1	23.23	24.92	24.62	15.69	19.38
2	22.54	29.54	27.46	14.77	23.00
3	22.62	28.80	17.08	15.46	25.08
4	23.85	28.54	28.92	17.37	25.38
5	24.23	28.31	29.92	17.77	26.92

Hence, the the best setting of the classifier are

- 25 selected features
- kernel order three
- the data collected at the position S2

With this setting the total accuracy of the classifier applied in different vehicles and different suspensions with variant loads is above 84.83%. Cause the limitation of the time and computing resource, the data may not be enough for a comprehensive training. But it is believed that with more variations, detailed parameters and longer simulation the accuracy of the classifier still has the potential to improve.

7. Summary and outlook

In this thesis, the full car model with 7 DOF is implemented to simulate the vibration of the vehicle caused by road infrastructure. Different models of road features e.g. pothole, manhole cover, railway crossing and cobbled road as well as the components of the vehicle such as the anti-roll bar and active suspension have been investigated and developed to expand the diversity of data for machine learning. Besides, the representation of the full car model has been converted from the state space to the transfer function, which makes the analysis of the inputs to any single output in frequency domain easier. To describe the complicated contact between the road and tire, several commonly used tire models have been analysed and a concise way has been found: a modified point contact tire model which is relative to the vehicle velocity and the length of obstacles.

After the identification of parameters the results of simulation match the actual measured data accurately and show a reasonable behavior in different situations. Then several representative features have been extracted to simplify and divide the data which is simulated by different vehicles traversing different roads into different dimensions. Additionally, the loads, vehicles and suspensions are also regarded as the input of the classification. Following this, different classifiers have been trained and tested by the simulated data and the corresponding ground truth. Furthermore, the possibility of the application of the classifier on different vehicles has been analyzed. Moreover, the influence of the variations e.g. the number of selected feature, the kernel order and the position of the output have also been investigated.

With the comparison of the simulated results to the measured results the full car model and road model are proved to be valid. Thus the data simulated from the model shall also be effective and could be applied in the machine learning. From the results of the simulation with different situations it is proved that the data processing method using inertial sensors has a good performance in the road infrastructure monitoring. The data can be good classified with different selected features and the accuracy of the classifier which is trained and tested by the data in the same condition is very high ($> 90\%$). With respect to the application, the classifier trained with the data of all variations reaches a relative high accuracy ($> 84\%$) regardless the variant loads on the vehicle, the type of the chassis or the model of vehicles.

Even though some good results have been achieved in the simulation, it is still essential to validate the accuracy of the classifier with the real measured data. In case that the result of measured data is not as good as the simulation, introducing more signals e.g. the accelerations of the wheels and extracting new features in time and frequency domain even the stiffness and damping ratios of the suspension etc. as well as expanding the variation or scale of the simulation may be a solution to improve the accuracy of the classifier. Besides, further improvements of the model could be completed to make the simulation more detailed and accurate. As to the investigation of the full car model, the center of the gravity, pitch and roll are assumed to be coincide in one point, which ignores the additional pitch- and roll moment caused by the vehicle body. Due to the cost and time of this work, the rigid ring tire model has not been implemented into the full car model. The tire model which considers not only the vertical also longitudinal dynamic has been shown to perform better and remain robust in the simulation of vertical spindle force.

A. List of Figures

Figure 2.1.	Generated road profile for simulation of car models described in Sections 2.4 to 2.6. Left and right profiles are different to investigate the influence of the anti-roll bar.	5
Figure 2.2.	Generated road profile for simulation of car models described in Sections 2.4 to 2.6. Left and right profiles are different to investigate the influence of the anti-roll bar.	5
Figure 2.3.	The strut equivalent schematic	6
Figure 2.4.	Full car model for simulation.	8
Figure 2.5.	Bode Phase Plot of All Transfer Functions.	11
Figure 2.6.	Coherence of the response between MIMO- and SISO system	12
Figure 2.7.	Model of anti-roll bar as a torsion bar between two unsprung masses. . . .	13
Figure 2.8.	Influence of the anti-roll bar. The roll acceleration is distinct reduced as well as the magnitude of the transfer function for lower frequencies.	14
Figure 2.9.	One fourth of the full car model with active suspension.	15
Figure 2.10.	Block diagram of the LQR.	16
Figure 2.11.	Control configuration of H_∞ control.	18
Figure 2.12.	Closed loop of H_∞ control.	19
Figure 2.13.	Bode plot of weighting functions W_{heave} , W_{roll} , W_{pitch} and W_{def}	20
Figure 2.14.	Influence of the active suspension on the vehicle dynamics.	21
Figure 2.15.	Body acceleration at different positions of the vehicle body.	24
Figure 2.16.	Rigid ring model.	26
Figure 2.17.	Contact situation with a short pothole.	29
Figure 3.1.	Geometric of the tire and speed bump.	31
Figure 3.2.	Profile of the simulated speed bump.	32
Figure 3.3.	Comparison of the vehicle response to a speed bump.	32
Figure 3.4.	Comparison of the standard deviation σ of vertical acceleration, roll rate and pitch rate between real measurement and simulated results.	34

Figure 4.1. Overview of the method to predict road features of class K_i based on vehicle dynamic data from simulation.	37
Figure 6.1. Classes separated by two aggregated features from 15 single features. . .	51
Figure 6.2. The classification with best 3 features of different suspensions	53
Figure 6.3. Influence of different position on the accuracy of the classification.	56

B. List of Tables

Table 2.1.	Definition of the variables	7
Table 2.2.	Parameter of the simulation	14
Table 2.3.	Position of outputs.	23
Table 2.4.	Ride phase tire model ranking via vertical acceleration [15].	25
Table 3.1.	Stiffness and damping ratio of the full car model.	33
Table 3.2.	Parameters for K and size of different events.	33
Table 4.1.	Example of a confusion matrix	40
Table 4.2.	Parameter of 3 vehicles	41
Table 6.1.	Confusion matrix of the training with BMW 116d passive suspension	51
Table 6.2.	Performance of classifiers for different vehicles.	52
Table 6.3.	Performance of the classifier for BMW 116d applied on different vehicles.	54
Table 6.4.	Confusion matrix of the training with all variations	55
Table 6.5.	Testing results of the classifier of all variations	55
Table 6.6.	Missclassification of application in BWM 116d with passive suspension	56
Table 6.7.	Missclassification of application in BWM 116d with anti-roll bar	56
Table 6.8.	Missclassification of application in BWM 116d with active suspension	57
Table 6.9.	Missclassification of application in S-Klasse W220 with passive suspension	57
Table 6.10.	Missclassification of application in Sprinter with passive suspension	57

Bibliography

- [1] ISO 8608. *Mechanical vibration - Road surface profiles - Reporting of measured data*, 2016.
- [2] A. Agharkakli, G. S. Sabet, and A. Barouz. Simulation and analysis of passive and active suspension system using quarter car model for different road profile. 2012.
- [3] M. Agostinacchio, D. Ciampa, and S. Olita. The vibrations induced by surface irregularities in road pavements – a Matlab® approach. *European Transport Research Review*, 6(3):267–275, Sept. 2014.
- [4] E. Alpaydin. *Introduction to Machine Learning*. MIT Press, 2014.
- [5] J. Barrand and J. Bokar. Reducing tire rolling resistance to save fuel and lower emissions. *SAE International Journal of Passenger Cars-Mechanical Systems*, 1(2008-01-0154):9–17, 2008.
- [6] M. L. Bermingham, R. Pong-Wong, A. Spiliopoulou, C. Hayward, I. Rudan, H. Campbell, A. F. Wright, J. F. Wilson, F. Agakov, P. Navarro, et al. Application of high-dimensional feature selection: evaluation for genomic prediction in man. *Scientific reports*, 5, 2015.
- [7] BMVI. Statistik des Lärmschutzes an Bundesfernstraßen 2014. Technical report, Bundesministerium für Verkehr und digitale Infrastruktur, Bonn, 2015.
- [8] D. Cebon and D. Cebon. *Handbook of Vehicle-Road Interaction*. Lisse ; Abingdon : Swets & Zeitlinger, 1999.
- [9] K. Chen, M. Lu, G. Tan, and J. Wu. CRSM: Crowdsourcing Based Road Surface Monitoring. In *High Performance Computing and Communications & 2013 IEEE International Conference on Embedded and Ubiquitous Computing (HPCCEUC), 2013 IEEE 10th International Conference On*, pages 2151–2158, 2013.
- [10] R. Darus and Y. M. Sam. Modeling and control active suspension system for a full car model. In *2009 5th International Colloquium on Signal Processing Its Applications*, pages 13–18, March 2009.

- [11] G. Descornet. Road-surface influence on tire rolling resistance. In *Surface characteristics of roadways: international research and technologies*. ASTM International, 1990.
- [12] M. Doody. Design and development of a composite automotive anti-roll bar. 2013.
- [13] J. Eriksson, L. Girod, B. Hull, R. Newton, S. Madden, and H. Balakrishnan. The Pothole Patrol: Using a Mobile Sensor Network for Road Surface Monitoring. In *Proceedings of the 6th International Conference on Mobile Systems, Applications, and Services*, pages 29–39. ACM, 2008.
- [14] Forschungsgesellschaft für Strassen- und Verkehrswesen. *Merkblatt über den Finanzbedarf der Straßenerhaltung in den Gemeinden*. FGSV-Verlag, 2004.
- [15] N. Frey. *Development of a Rigid Ring Tire Model and Comparison Among Various Tire Models for Ride Comfort Simulations*. BiblioBazaar, 2012.
- [16] I. Guyon and A. Elisseeff. An introduction to variable and feature selection. *Journal of machine learning research*, 3(Mar):1157–1182, 2003.
- [17] A. Ihs. The influence of road surface condition on traffic safety and ride comfort. In *6th International Conference on Managing Pavements 19–24 October 2004. Brisbane Convention & Exhibition Centre, Queensland Australia.*, pages 11–21. Statens väg-och transportforskningsinstitut, 2005.
- [18] V. Iliev. *Systemansatz zur anregungsunabhängigen Charakterisierung des Schwingungskomforts eines Fahrzeugs*. Karlsruher Institut für Technologie, 2014.
- [19] R. Isermann. *Mechatronische systeme: Grundlagen*. Springer-Verlag, 2007.
- [20] R. N. Jazar. *Vehicle dynamics. Theory and Applications*. Riverdale, NY: Springer Science+Business Media, 2008.
- [21] M. Kaleemullah, W. F. Faris, and F. Hasbullah. Design of robust h, fuzzy and lqr controller for active suspension of a quarter car model. In *2011 4th International Conference on Mechatronics (ICOM)*, pages 1–6, May 2011.
- [22] C. Koch and I. Brilakis. Pothole detection in asphalt pavement images. *Advanced Engineering Informatics*, 25(3):507–515, 2011.
- [23] J. Masino, B. Wohnhas, M. Frey, and F. Gauterin. Identification and Prediction of Road Features and their Contribution on Tire Road Noise. *WSEAS Transactions on Systems and Control*, 12:201–212, 2017.

- [24] Control system toolbox: Design and analyze control systems. <https://www.mathworks.com/products/control.html>.
- [25] Scixminer: Open-source matlab toolbox for multidimension data mining. <https://sourceforge.net/projects/scixminer/>.
- [26] Robust control of an active suspension. <https://de.mathworks.com/help/robust/gs/active-suspension-control-design.html>.
- [27] Signal processing toolbox: Perform signal processing and analysis. <https://de.mathworks.com/help/signal/index.html>.
- [28] R. Mikut, A. Bartschat, W. Doneit, J. Á. G. Ordiano, B. Schott, J. Stegmaier, S. Waczowicz, and M. Reischl. The matlab toolbox scixminer: User's manual and programmer's guide. *arXiv preprint arXiv:1704.03298*, 2017.
- [29] S. Na, D. Park, and W. Yoo. Rigid ring with bouc–wen tire model for vehicle dynamic analysis. *Proceedings of the Institution of Mechanical Engineers, Part C: Journal of Mechanical Engineering Science*, page 0954406216647416, 2016.
- [30] H. M. Ngwangwa, P. S. Heyns, F. J. J. Labuschagne, and G. K. Kululanga. Reconstruction of Road Defects and Road Roughness Classification Using Vehicle Responses with Artificial Neural Networks Simulation. *Journal of Terramechanics*, 47(2):97–111, Apr. 2010.
- [31] P. Nitsche, R. Stütz, M. Kammer, and P. Maurer. Comparison of Machine Learning Methods for Evaluating Pavement Roughness Based on Vehicle Response. *Journal of Computing in Civil Engineering*, 28(4):04014015, 2012.
- [32] E. Öhrström, A. Skanberg, H. Svensson, and A. Gidlöf-Gunnarsson. Effects of Road Traffic Noise and the Benefit of Access to Quietness. *Journal of Sound and Vibration*, 295(1):40–59, 2006.
- [33] S. C. Radopoulou and I. Brilakis. Automated Detection of Multiple Pavement Defects. *Journal of Computing in Civil Engineering*, page 04016057, 2016.
- [34] S. C. Radopoulou and I. Brilakis. Improving Road Asset Condition Monitoring. *Transportation Research Procedia*, 14:3004–3012, 2016.
- [35] D. Sammier, O. Senname, and L. Dugard. Skyhook and h8 control of semi-active suspensions: Some practical aspects. *Vehicle System Dynamics*, 39(4):279–308, 2003.
- [36] U. Sandberg. Road traffic noise—The influence of the road surface and its characterization. *Applied Acoustics*, 21(2):97–118, Jan. 1987.

- [37] S. M. Savaresi, C. Poussot-Vassal, C. Spelta, O. Sename, and L. Dugard. *Semi-active suspension control design for vehicles*. Elsevier, 2010.
- [38] D. H. Schwela. The World Health Organization Guidelines for Environmental Noise. *Noise News International*, 8(1):9–22, 2000.
- [39] F. Seraj, B. J. van der Zwaag, A. Dilo, T. Luarasi, and P. Havinga. RoADS: A Road Pavement Monitoring System for Anomaly Detection Using Smart Phones. In *Big Data Analytics in the Social and Ubiquitous Context*, pages 128–146. Springer, Cham, Apr. 2014.
- [40] A. Shariati, H. Taghirad, and A. Fatehi. Decentralized robust h controller design for a half-car active suspension system. *Proceedings of Control 2004*, pages 1–5, 2004.
- [41] M. Sokolova and G. Lapalme. A systematic analysis of performance measures for classification tasks. *Information Processing Management*, 45(4):427 – 437, 2009.
- [42] S. M. Taylor, B. E. Breston, and F. L. Hall. The effect of road traffic noise on house prices. *Journal of Sound and Vibration*, 80(4):523–541, Feb. 1982.
- [43] M. A. J. Theebe. Planes, Trains, and Automobiles: The Impact of Traffic Noise on House Prices. *The Journal of Real Estate Finance and Economics*, 28(2):209–234, 2004.
- [44] Reifenrechner: Reifen- und reifenhaendler suchmaschine fuer deutschland. https://www.reifensuchmaschine.de/reifen_rechner/.
- [45] H. Wallentowitz. *Vertikal-, Querdynamik von Kraftfahrzeugen: Federungssysteme, Fahrverhalten, Lenkung, Radaufhängung ; Vorlesungsumdruck Fahrzeugtechnik II*. Schriftenreihe Automobiltechnik. Forschungsges. Kraftfahrwesen, 1997.
- [46] C. C. Ward and K. Iagnemma. Speed-independent vibration-based terrain classification for passenger vehicles. *Vehicle system dynamics*, 47(9):1095–1113, 2009.
- [47] M. Wilhelmsson. The Impact of Traffic Noise on the Values of Single-family Houses. *Journal of Environmental Planning and Management*, 43(6):799–815, Nov. 2000.
- [48] P. W. A. Zegelaar. The dynamic response of tyres to brake torque variations and road unevennesses. 1998.